

Model guided development of astaxanthin production in microalgae biofilms

David Morgado, Andrea Fanesi, Benoit Chachuat, Sihem Tebbani, Olivier Bernard, Filipa Lopes

▶ **To cite this version:**

David Morgado, Andrea Fanesi, Benoit Chachuat, Sihem Tebbani, Olivier Bernard, et al.. Model guided development of astaxanthin production in microalgae biofilms. Algal Research - Biomass, Biofuels and Bioproducts, 2025, 91, pp.104201. ⟨10.1016/j.algal.2025.104201⟩. ⟨hal-05289754⟩

HAL Id: hal-05289754

https://hal.science/hal-05289754v1

Submitted on 30 Sep 2025

HAL is a multi-disciplinary open access archive for the deposit and dissemination of scientific research documents, whether they are published or not. The documents may come from teaching and research institutions in France or abroad, or from public or private research centers.

L'archive ouverte pluridisciplinaire **HAL**, est destinée au dépôt et à la diffusion de documents scientifiques de niveau recherche, publiés ou non, émanant des établissements d'enseignement et de recherche français ou étrangers, des laboratoires publics ou privés.



Distributed under a Creative Commons CC BY 4.0 - Attribution - International License

Algal Research 91 (2025) 104201



Contents lists available at ScienceDirect

Algal Research

journal homepage: www.elsevier.com/locate/algal





Model guided development of astaxanthin production in microalgae biofilms☆

David Morgado [a], Andrea Fanesi [a,*], Benoit Chachuat [b], Sihem Tebbani [c], Olivier Bernard [d], Filipa Lopes [a]

[a] Université Paris-Saclay, CentraleSupélec, Laboratoire Génie des Procédés et Matériaux (LGPM), Gif sur Yvette, France
[b] The Sargent Centre for Process Systems Engineering, Department of Chemical Engineering, Imperial College London, London, United Kingdom
[c] Université Paris-Saclay, CentraleSupélec, CNRS, Laboratoire des Signaux et Systèmes (L2S), Gif sur Yvette, France
[d] INRIA, Centre d'Université Côte d'Azur, GreenOwl, Sophia-Antipolis, France

ARTICLE INFO

Keywords:
Haematococcus lacustris
Biofilm
Astaxanthin
Modeling
Optimization
Microalgae

ABSTRACT

Biofilm systems present a promising approach for microalgae production by reducing water and energy costs while improving productivity and operational efficiency. However, this technology is still in its infancy, particularly for high-value compounds production. To confirm its potential at large scale, mathematical models are required to better understand biofilm behavior under varying environmental conditions and to predict productivity. In this study, a dynamic model was developed to estimate astaxanthin production by *Haematococcus lacustris* biofilms on a rotating system. It incorporates well-established dynamics, accounting for nitrogen limitation and photoacclimation, while introducing a novel hypothesis correlating astaxanthin dynamics with those of chlorophyll. The model predicts key biofilm traits, including biomass density, intracellular nitrogen, and pigment quotas, demonstrating its ability to simulate changes in light and nitrogen conditions and assess their impact on biofilm physiology. Furthermore, the possibility of dynamically altering the life cycle of *H. lacustris* within a biofilm was demonstrated both experimentally and mathematically, enabling reversible transitions between green and red stages. This reversion facilitates continuous astaxanthin production through repeated harvest and regrowth cycles. This was assessed through the development of an optimization strategy that maximized astaxanthin productivity by adjusting light intensity over time and determining the optimal harvest frequency. The model provides a valuable framework for optimizing astaxanthin production in microalgal biofilms, enabling the development of continuous production systems and supporting the scale-up of biofilm technology.

1. Introduction

Microalgae are photosynthetic organisms that thrive under fluctuating environmental conditions such as light, nutrients, and temperature. They display remarkable physiological plasticity, adjusting their physiological profile to environmental changes from minutes to seasons by actively modifying photosynthesis and their biochemical compositions, such as pigment, protein, lipid or carbohydrate contents [1].

Depending on the timescale of these biological changes, three processes can be distinguished: regulation (seconds/min), acclimation (days) and adaptation (over years) [2]. Based on the duration of most experimental studies (laboratory and field studies), the adjustments that cells undergo when challenged with varying growth conditions can be identified as acclimation strategies enacted by the cells to reduce damage and maximize their fitness under the new conditions [3]. Acclimation, under excessive excitation pressure, includes the *de-novo* synthesis of macromolecules such as carotenoids, polyunsaturated fatty acids, and polysaccharides, making microalga and its bio-products valuable for various biotechnological applications [4].

Among the plethora of macromolecules produced by microalgae to cope with stressful conditions, astaxanthin is a carotenoid that can be naturally produced by exploiting the physiology of *Haematococcus lacustris*, a green alga that can accumulate up to 5 % of its dry weight in astaxanthin. Due to this ability, it has become the primary commercial

☆ This article is part of a Special issue entitled: 'DigitAlgaesation' published in Algal Research.

* Corresponding author.
E-mail address: andrea.fanesi@centralesupelec.fr (A. Fanesi).

https://doi.org/10.1016/j.algal.2025.104201
Received 31 March 2025; Received in revised form 3 July 2025; Accepted 6 July 2025
Available online 14 July 2025
2211-9264/© 2025 The Authors. Published by Elsevier B.V. This is an open access article under the CC BY license (http://creativecommons.org/licenses/by/4.0/).

source of natural astaxanthin [5]. The industrial standard commonly follows a two-stage process, where biomass grows under optimal conditions (green stage), usually in closed photobioreactors, followed by a red stage, where astaxanthin production is induced via stress conditions such as high irradiance and nitrogen starvation, and potentially temperature, salinity, and desiccation [6,7]. Numerous production facilities have been established worldwide, varying in production scales and cultivation methodologies, and consequently, in production costs [8]. However, the cost of production remains nearly four times that of chemical synthesis, which accounts for 95 % of commercially produced astaxanthin, primarily due to the substantial energy required [9]. This highlights a critical need for innovation in this area.

One potential cost-reducing technology is the use of biofilm-based systems for microalgae cultivation. In such systems, biomass is immobilized and decoupled from the liquid medium reducing water and energy costs [10]. Recent research has demonstrated the feasibility of producing astaxanthin through biofilm technology [11–16]. Since biofilms per definition display great spatial heterogeneity, complicating direct measurements and control, optimizing and controlling these systems is an essential step for making such technologies economically relevant. Thus, mathematical models might be pivotal in understanding and predicting the complex behavior of biological processes within biofilms and developing strategies to enhance productivity without extensive experimental work by simulating "what if" scenarios [17,18].

Such models typically compute microalgae growth as dependent on external stimuli such as light intensity, nutrients concentration and temperature. Models accounting for acclimation processes make them more accurate for changing environmental conditions. Indeed, while stress can induce the production of desired compounds, it often comes at the cost of a decreased biomass growth rate [19]. Therefore, modeling the rates of nutrient assimilation, photosynthesis, and pigment synthesis during transient regimes is crucial, especially when exploiting these microorganisms for biotechnological purposes.

Several dynamic models describe planktonic microalgae growth [20–22] but similar models for microalgal biofilms are scarce. While bacterial biofilm models have been extensively studied and applied in wastewater treatment [23,24], only a few models integrate both microalgal physiology and biofilm dynamics. Such approaches typically involve complex frameworks that include spatial discretization, such as in Porous Substrate Bioreactors (PSBR) [25,26], two-dimensional (2D) cellular automata models [27,28] and 2D mixture theory models describing metabolic compartments within the biofilm [29].

When modeling molecules such as astaxanthin, specific physiological considerations must be accounted for. Astaxanthin synthesis can be independently triggered by either high-light intensity or nitrogen starvation, but only the combination of both stresses results in a maximum physiological limit of astaxanthin content [6,30]. These stresses impact the photosynthetic efficiency and elemental composition of *H. lacustris*, disrupting the photosynthetic apparatus and chlorophyll biosynthesis, leading to the accumulation of macromolecules such as starch and lipids [31]. Existing models, primarily available for planktonic cultures, often use the Luedeking-Piret approach [32] of growth and non-growth-linked product accumulation [33–35], including for *Chromochloris zofingiensis* [36]. These models do not account for intracellular nitrogen and carbon quotas, nor do they consider photoacclimation and chlorophyll dynamics. To date, only the study of Zhang et al. [37] has modeled astaxanthin production in an attached cultivation system, incorporating intracellular nitrogen quota and temperature dynamics. Their experimental design, however, relied on fixed incident light intensity and nitrogen-depleted conditions, utilizing a PSBR with a microfiltration membrane, which presents scale-up limitations [12,13] recently explored the cultivation of *H. lacustris* in rotating systems, which are considered easier to scale up and provide a "greener" and more cost-efficient alternative to traditional photobioreactors [38,39]. Although these systems have been modeled, their primary applications have been in wastewater treatment and mixed communities, or solely for biomass production, rather than for high-value compounds [40,41].

Based on these observations, we develop a dynamic model for quantitative prediction of astaxanthin production. The model describes the life cycle of *H. lacustris* biofilms, including transitions from the green to the red stage and vice versa, under varying light and nitrogen stresses. It integrates well-established dynamics from planktonic models, such as the Droop model and photoacclimation concepts [21,42], while introducing a novel hypothesis that correlates the dynamics of astaxanthin with those of chlorophyll. Also, it accounts for light attenuation due to the rotating system and variations in photosynthetic photon flux density (PPFD) across the biofilm depth. The model is calibrated against robust elemental composition measurements, in terms of biomass density, intracellular nitrogen, chlorophyll-*a* and astaxanthin quotas. The detailed representation of physiological changes within each biofilm layer, coupled with the reversibility of the life cycle, makes this model suitable for developing optimization strategies. Such strategies are briefly explored to identify optimal harvesting frequencies and light conditions that maximize astaxanthin productivity.

2. Experimental setup

2.1. Experimental design

A detailed description of the experimental design and of the rotating biofilm cultivation system is reported in Morgado et al. [13] and is summarized in Table 1. In brief, *Haematococcus lacustris* (strain CCAC 0125; Central collection of algal cultures, University of Duisburg-Essen, Cologne, Germany) biofilms were cultivated on cotton carriers within a rotating biofilm-based system consisting of 4 cylinders, each with a working volume (V) of 1-L and a biofilm growth area (A) of 0.0396 m^2. Pure cotton was preferred to other fabric materials due to its natural origin and absence of synthetic fibers. The initial inoculum of planktonic culture of 0.33 g L^{-1} and each cylinder operated at a linear velocity of 0.0346 m s^{-1} (6 rpm), meaning that the biofilm is exposed 5 s to air and 5 s submersed.

Briefly, a two-stage cultivation strategy for astaxanthin production was employed, utilizing different reactors under varying photon flux densities and nitrogen regimes for 15 days. During the first 7 days of each experiment, all reactors were maintained under replete nitrogen conditions (green stage). Two reactors were exposed to a photosynthetic photon flux density (PPFD) of 50 μmol m^{-2} s^{-1}, while the other two were exposed to a PPFD of 200 μmol m^{-2} s^{-1}. After 7 days, the PPFD was increased in all reactors to a fixed level of either 400 or 800 μmol m^{-2} s^{-1}. At this point, the medium of the two reactors was changed to a nitrogen-deplete condition (red stage), while the other two were maintained under replete nitrogen conditions (N-replete). An additional experiment was conducted to assess the feasibility of reverting from the red stage to the green stage. After growing the biofilms for 14 days, 7 days under the condition of 200 μmol m^{-2} s^{-1} (green stage) and 7 days

Table 1
Experimental design for model estimation and validation, including datasets from [13] and reversion of the red to green stage.

Stages	Light Intensity (PPFD)		N-condition[a]	Model
	Initial	Final		
Only Green Stage	50	400	N+	Estimation
	200	400	N+	Estimation
	50	800	N+	Validation
	200	800	N+	Estimation
Green to Red Stage	50	400	N-	Estimation
	50	800	N-	Estimation
	200	800	N-	Estimation
Reversion	200	400	N-/N+	Validation

[a] N+ represent the growth medium (Bristol) with the normal Nitrate concentration. N- represents the Bristol medium without Nitrate to stimulate the red stage.

under 400 μmol μmol m^{-2} s^{-1} N-deplete (red stage), nutrients were reintroduced into the system while the light intensity was maintained at 400 μmol m^{-2} s^{-1}. Biofilm traits were monitored over the subsequent 7 days, and the experimental results were compared with the model's predictions.

2.2. Rotating system and dark-light cycles

Cultivation strategies such as constant light or dark-light cycles can positively or negatively influence growth rates. A rotating system represents a strategy where implementing these cycles may mitigate photodamage by temporally diluting light exposure, allowing microalgae cells to experience alternating light/dark (L/D) cycle [43–45]. In this study, the rotating biofilm-based system was operated at 6 rpm [13], which means a time-cycle of 10 s for light. According to Fierro Ulloa et al. [46], growth rate can be averaged in time and expressed as a function of the average PPFD. Moreover, Combe et al. [47] suggests that under fluctuating light conditions, chlorophyll content is primarily influenced by average light intensity rather than peak levels. Here, we discuss the model assuming that incident PPFD (I_0) is averaged over the duty cycle, π, represented from now on as $\overline{I_0} = I_0/\pi$ (Fig. S1, Eq. S1 and S2).

3. Model development

The mathematical model for astaxanthin production in microalgae biofilms comprises a set of equations describing the dynamics of six state variables, quantified either in terms of mass concentration of carbon (C) or nitrogen (N) (Table 2).

The model is designed assuming the following (Fig. 1 and Table 2):

1. The establishment of the biofilm begins with an initial adhesion phase independent of the light intensity, where cells transition from the planktonic culture (x_L) to the cotton carriers, governed by a physical constant, k (adhesion rate), eq. (1).
2. The model represents the biofilm thickness (h), assuming a constant and uniform carbon-specific biofilm density (ρ_C) across the biofilm matrix on the cotton carrier. This implies that the biomass grows uniformly along the vertical axis, with a fixed area. Consequently, the relationship between biomass X (in terms of C) and biofilm thickness (h) can be expressed as $h = X/\rho_C$. The second term of the equation $\left(k{\cdot}x_L\frac{V}{A}\right)$ accounts for the transfer of biomass from the planktonic culture to the cotton carriers.
3. The carbon-specific gross growth rate (μ) is dependent on the average PPFD $\left(\overline{I_0} = I_{0/\pi}\right)$, chlorophyll-$a$ quota (θ) (which varies with biofilm depth) and intracellular nitrogen quota (q) following the Droop Model, (Fig. 1A).
4. The loss of biomass is represented by a single respiration term (R), which occurs continuously and independently of light or carbon synthesis. The net growth rate becomes negative when the light intensity received by cells within the biofilm falls below the light compensation point. At the minimum intracellular nitrogen quota (q_{min}) or when light intensity is zero, the net growth rate equals $-R$ (Fig. 1A).
5. The substrate uptake rate follows Michaelis-Menten kinetics, down-regulated by the nitrogen quota (q), and q is constant over the biofilm depth (Fig. 1B).
6. Chlorophyll-a quota (θ) is proportional to the intracellular nitrogen quota (q) with a coefficient of proportionality that is a decreasing function of the PPFD (I) (Fig. 1C). It is therefore increasing with depth.
7. Astaxanthin quota (w) is described as a function of chlorophyll-a (θ) at equilibrium (Fig. 1D).

3.1. Light irradiance

Photosynthetic cultivation systems rely on light transfer, affecting growth kinetics. In planktonic cultures, light absorption is primarily determined by the fraction of photosynthetic pigments in the biomass and cell scattering [48]. The behavior of light in suspensions and biofilms is similar. However, biofilms have unique properties like denser structure, extracellular polymeric substances (EPS), less water content, and shorter light path. Therefore, the scattering term can generally be disregarded, with the biofilm thickness causing the most significant attenuation, with minimal contribution of pigments [49]. Therefore, light attenuation in biofilms is modeled using the Beer-Lambert Law with a single parameter for the extinction coefficient (ϵ), where the average incident PPFD ($\overline{I_0}$, diluted by the duty cycle) decreases with depth z, with z always being a negative value from $z \in [-h, 0]$:

$$I(z) = \overline{I_0}{\cdot}e^{\epsilon z} \tag{7}$$

3.2. Droop model and substrate uptake

The Droop Model [50,51] is a well-established framework for predicting microalgal dynamics behavior under nitrogen-limited conditions [52]. The model highlights that microalgae can continue to grow even after the limiting nutrient (S) in the liquid has been depleted, requiring a minimum intracellular nitrogen quota (q_{min}) of nutrients for growth to occur. The rate of change of the internal concentration of nitrogen is described as the difference between nitrogen assimilation and remineralization (Supplementary Materials).

$$\dot{q} = r_S(S,q) - \overline{\mu}(h,q)q \tag{8}$$

The carbon-specific nitrogen uptake rate (r_S) is driven by the Michaelis-Menten kinetics of the dissolved inorganic nitrogen concentration (S). It is assumed to decrease with the intracellular nitrogen quota and to stop upon reaching q_{max}.

$$r_S\left(S,q\right) = r_{S_{max}}\frac{S}{S+K_S}\left(\frac{q_{max}-q}{q_{max}-q_{min}}\right) \tag{9}$$

Table 2
Model state variables, initial conditions and dynamic equations.

State Variables	Init. Cond.	Units	Dynamic Equations	
Planktonic Cells in Liquid Phase (x_L)	330	$g_C\ m^{-3}$	$\dot{x_L} = -k{\cdot}x_L$	(1)
Biomass Areal Density in Biofilm (X)	1.25	$g_C\ m^{-2}$	$\dot{X} = [\overline{\mu}(h,q) - R]X + k{\cdot}x_L\frac{V}{A}$	(2)
Substrate Concentration (S)	100	$g_N\ m^{-3}$	$\dot{S} = -r_S\left(S,q\right)\left(X\frac{A}{V} + x_L\right)$	(3)
Internal Nitrogen Quota (q)	0.13	$g_N\ g_C^{-1}$	$\dot{q} = r_S(S,q) - \overline{\mu}(h,q)q$	(4)
Chlorophyll-a Quota (θ)	0.028	$g_{Chl\text{-}a}\ g_C^{-1}$	$\dot{\theta} = \delta_\theta[\overline{\theta}(h,q) - \theta]$	(5)
Astaxanthin Quota (w)	0.0025	$g_{Astx}\ g_C^{-1}$	$\dot{w} = \delta_w[\overline{w}(h,q) - w]$	(6)

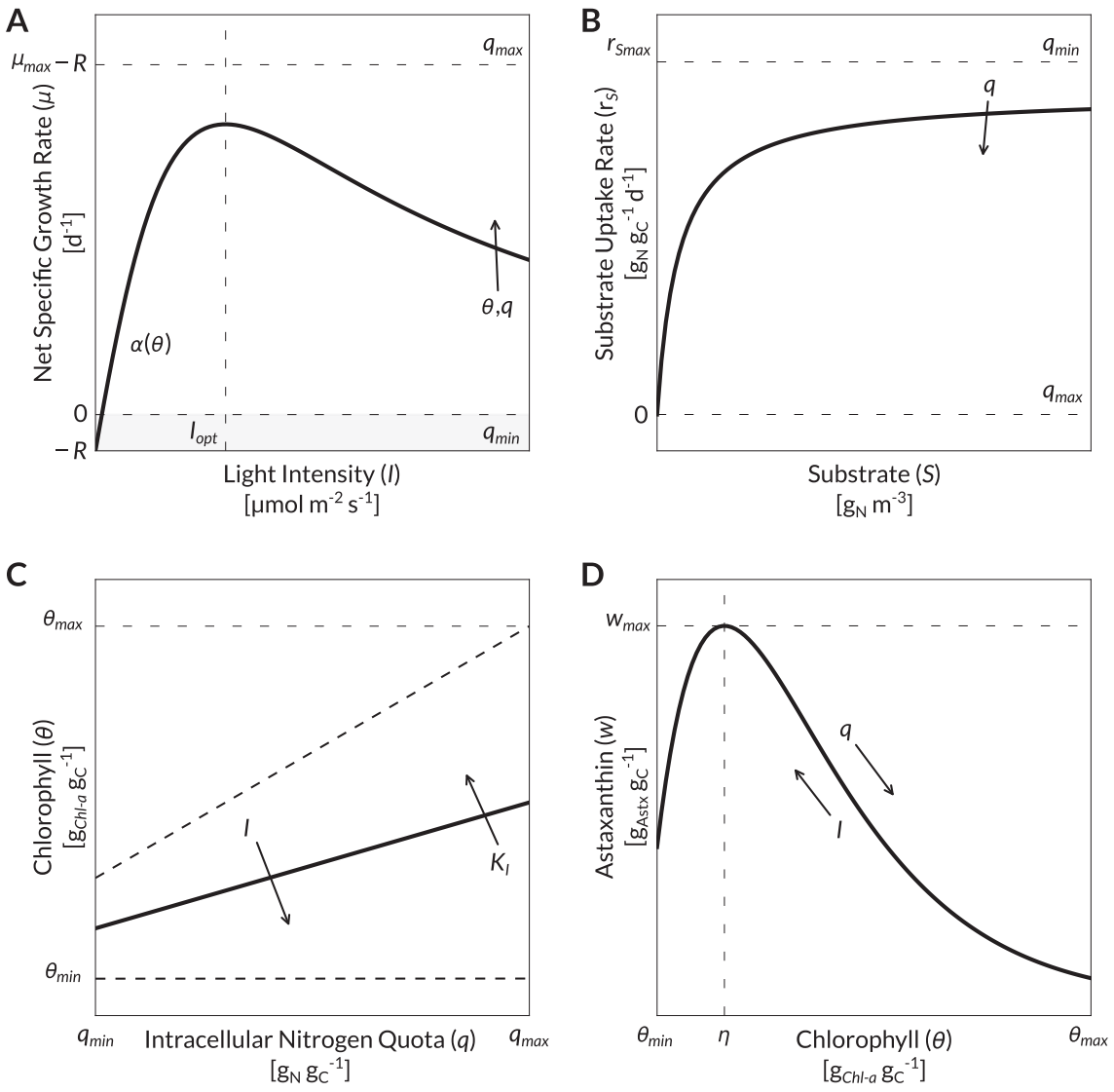


Fig. 1. Graphical summary of the dependencies of net growth rate ($\mu - R$), nitrogen assimilation (r_S), chlorophyll-*a* quota (θ), and astaxanthin quota (w) dynamics on environmental and physiological variables. (A) The net growth rate represents the balance between carbon-specific growth μ and respiration (R) rates. It is defined as a Haldane-type function of PPFD (I), intracellular nitrogen quota (q), and chlorophyll-a quota (θ). This function is parameterized by the initial slope ($\alpha^{Chl}\theta$) and the $\widetilde{\mu}$ that yields the maximum growth rate μ_{max}) at the maximum intracellular nitrogen quota (q_{max}) under optimal light PPFD (I_{opt}). The net growth rate becomes negative when the light intensity received by cells within the biofilm falls below the light compensation point. At the minimum intracellular nitrogen quota (q_{min}) or when light intensity is zero, the net growth rate equals $-R$. (B) The carbon-specific nitrogen assimilation rate (r_S) is assumed to be driven by the Michaelis-Menten kinetics of the dissolved inorganic nitrogen concentration (S), parameterized by a maximum nitrogen uptake rate ($r_{S_{max}}$). The maximum uptake rate occurs at q_{min} and is downregulated at higher values until it ceases at q_{max}. (C) Chlorophyll-*a* quota (θ) is proportional to the intracellular nitrogen quota (q) with a coefficient of proportionality that is a decreasing function of PPFD (I). This function is parameterized by species-dependent parameters: a light inhibition coefficient (K_I) and a chlorophyll-*a* yield (γ_m). θ_{min} is found at high I and q_{min}, while θ_{max} is found at low I and q_{max}. (D) Astaxanthin quota (w) is a function of chlorophyll-*a* quota at equilibrium. It assumes that the effects of light and intracellular nitrogen quota on astaxanthin are similar to those on chlorophyll. It describes that when stress conditions are too high (reaching a θ_{min}), the cells do not have the available photosynthetic machinery to produce astaxanthin. Therefore, there is an optimal chlorophyll quota (η) where the astaxanthin quota is maximum. Basal levels of astaxanthin are detected at θ_{max}.

where $r_{S_{max}}$ [$g_N\ g_C^{-1}\ d^{-1}$] for sake of simplicity is equal to $\mu_{max} \times q_{max}$ [53,54], and K_S is the nitrogen half-saturation constant [$g\ m^{-3}$].

3.3. Growth rate

Net growth rate is given by the difference between growth and respiration. The growth rate is described as a function of PPFD (I) and intracellular nitrogen quota (q) by a Haldane-type equation [55]:

$$\mu(I(z),\theta(z),q) = \widetilde{\mu}\frac{I}{I + \frac{\widetilde{\mu}}{\alpha(\theta)}\left(\frac{I}{I_{opt}} - 1\right)^2}\left(1 - \frac{q_{min}}{q}\right) \quad (10)$$

parameterized by α, the initial slope of μ [d^{-1}], independent of the PPFD but dependent on the chlorophyll quota (θ) in a way that $\alpha(\theta) = \alpha^{Chl}\theta$ (α^{Chl} is the initial slope of a chlorophyll-specific growth rate) [56]; and by $\widetilde{\mu}$, which becomes μ_{max} when $q = q_{max}$ and $I = I_{opt}$, Fig. 1 and eq. (S9).

Experimental evidence from perfectly mixed photobioreactors suggests that photosynthetic efficiency increases with depth, implying that microalgae cells respond almost instantaneously to variations in light intensity [57–59]. In biofilms, where cells are immobilized, accurate modeling of the light intensity reaching each cell becomes critical for predicting the microalgae growth rate. Thus, the average growth rate, $\overline{\mu}(h,q)$ is calculated by integrating the local growth rate along the

biofilm's thickness h, ranging from the biofilm surface at $z = 0$ to the substrate at $z = -h$:

$$\overline{\mu}\left(h,q\right) = \frac{1}{h}\int_{-h}^{0}\mu\left(I\left(z\right),q\right)dz \tag{11}$$

3.4. Astaxanthin and chlorophyll dynamics

Microalgae can cope with varying light intensities by adjusting their photosynthesis response and their pigment content through photoacclimation. Specifically, cells acclimated to low irradiance exhibit a higher chlorophyll content compared to those acclimated to high irradiance, given the same intracellular nitrogen quota [56]. Additionally, the concentration of chlorophyll-a is closely linked to proteins within the pigment-protein complexes of the photosynthetic machinery [19]. Therefore, under nitrogen-depleted conditions, these complexes are significantly impaired.

Chlorophyll and nitrogen dynamics are tightly coupled with astaxanthin synthesis/degradation in *Haematococcus lacustris*. Experimental data and microscopy observations have shown an inverse correlation between the levels of astaxanthin in lipid bodies and chlorophyll [60–62], suggesting that the products from the degradation of chlorophyll may be utilized in the synthesis of astaxanthin [63]. Therefore, in this study, we model for the first time astaxanthin as a function of chlorophyll dynamics, based on the well-established understanding of chlorophyll photoacclimation dynamics. This methodology reduces the number of parameters needed for estimation, ensuring a direct and conservative relationship between the new dynamic equation and the documented mechanisms of chlorophyll synthesis, sharing the same dependencies on light and intracellular nitrogen quota.

Chlorophyll density (*Chl*) [*Chl-a* m^{-2}] once photoacclimated is assumed to be proportional to cellular proteins, represented by the particulate nitrogen *Xq* [64], with a proportionality factor $\gamma(I)$ depending on light intensity [64]. By introducing the chlorophyll quota (θ) (*Chl/X*) [*Chl-a* g_C^{-1}], this relationship can be formulated as:

$$\theta^{*} = \gamma(I)q \tag{12}$$

$$\gamma\left(I\right) = \gamma_m\frac{K_I}{I+K_I} \tag{13}$$

where K_I is a light inhibition constant [μmol m^{-2} s^{-1}], and γ_m is a chlorophyll-*a* yield term [*Chl*$_a$ g_N^{-1}] representing the capacity of nitrogen to support photosynthesis and growth [65].

The dynamics of θ are modeled as first-order dynamics where θ tends to adapt towards a steady state value (θ^{*}) influenced by a photoacclimation rate constant (δ_θ) [d^{-1}]; [21,52]. Since the biofilms are not in a steady state and pigment concentrations in each individual layer are not directly measurable, experimental data typically reflect the average pigment content across the biofilm. In biofilms, gradients of both chlorophyll and astaxanthin are observed across depth [16,66]. To account for this, we apply the same methodology used for calculating the average growth rate, Eq. (10), computing the chlorophyll quota across different layers of the biofilm and the subsequent average. By combining Eq. (11) and Eq. (12), we derive:

$$\overline{\theta}\left(h,q\right) = \frac{\gamma_m\cdot q}{h}\int_{-h}^{0}\frac{K_I}{I(z)+K_I}dz \tag{14}$$

$$\dot{\theta} = \delta_\theta(\overline{\theta}-\theta) \tag{15}$$

The astaxanthin quota (*w*) is modeled as a function of chlorophyll-*a* quota at equilibrium (Eq. (15), Fig. 1D). This assumes that the effects of light and intracellular nitrogen quota on astaxanthin are similar to those on chlorophyll, with an optimal chlorophyll-*a* quota (η) [$g_{Chl\text{-}a}$ g_C^{-1}] where the astaxanthin quota is maximal, as shown in Eq. (16).

$$w^{*} = \widetilde{w}\cdot\theta^{*}\cdot e^{-\frac{\theta^{*}}{\eta}} \tag{16}$$

$$w_{max} = \widetilde{w}\frac{\eta}{e} \tag{17}$$

Given the dynamic and non-steady state of the astaxanthin-chlorophyll relationship observed in vivo, we model the astaxanthin dynamics ($\dot{w}$) in a manner analogous to the chlorophyll dynamics ($\dot{\theta}$) presented in Eq. (14). The average astaxanthin quota, $\overline{w}(h,q)$ is computed using the chlorophyll quota derived from Eq. (13) and incorporated into Eq. (15). These dynamics are governed by a constant rate δ_w [d^{-1}], which accounts for both the stress-induced accumulation of astaxanthin and its degradation when environmental conditions become more favorable.

$$\dot{w} = \delta_w\left[\widetilde{w}\cdot\overline{\theta}\cdot e^{-\frac{\overline{\theta}}{\eta}} - w\right] \tag{18}$$

3.5. Parameter estimation and model validation

3.5.1. Parameter estimation

The experimental datasets that were collected under various cultivation conditions are partitioned into estimation and validation datasets (Table 1). The model predictions for the calibration set are reported in supplementary materials (Fig. S2–7).

The complete model comprises 15 parameters, of which 10 were estimated using maximum likelihood estimation (MLE) and statistical confidence analysis with gPROMS v7.0 software (Siemens Process Systems Engineering) [67]. These estimated parameters are grouped into the following categories:

- Intracellular nitrogen quota parameters: q_{min} and q_{max}
- Growth parameters: μ_{max}, I_{opt} and α^{Chl}
- Chlorophyll parameters: γ_m and K_I
- Astaxanthin parameters: $\widetilde{w}$, η and δ_w

The remaining six parameters were fixed based on experimental observations and literature values:

- Adhesion rate (*k*): Fixed at 0.17 d^{-1} based on the measured decrease in planktonic biomass concentration from 330 to 100 g_C m^{-3} over 7 days in this study;
- Photoacclimation rate (δ_θ): This rate has been reported to be proportional to the specific growth rate (μ) or as a constant positive value when microalgae are illuminated, and zero in the absence of light [68,69]. Here, δ_θ was set equal to μ_{max}. This choice aligns with the timescales of the photoacclimation process, implying a biological limit that cannot exceed the maximum growth rate, while the actual chlorophyll-related processes are regulated by the dynamics of light and intracellular nitrogen quota within the biofilm;
- Extinction coefficient (ϵ): The parameters α^{Chl} and ϵ cannot be determined independently. While the extinction coefficient is species-dependent in liquid cultures [70], it remains relatively conserved across biofilms (Table 3). Moreover, the extinction coefficient has also been estimated by measuring oxygen profiles within

Table 3
Extinction coefficient for different microalgae biofilms.

Species	Extinction Coefficient	References
Scenedesmus obliquus	2.12×10^4	[74]
Halochlorella rubescens	$2.0 - 3.5 \times 10^4$	[72]
Chlamydomonas reinhardtii	1.8×10^4	[75]
Chlorella vulgaris	11.6×10^4	[76]
Haematococcus lacustris	2.0×10^4	This work

the biofilm's depth. Studies by [71–73] demonstrated that oxygen production decreases as light intensity falls below the light compensation point. Therefore, we performed oxygen microprofiling experiments (Fig. S8 and S9) and determined the photosynthetically active zone of the biofilm for each incident light, estimating ϵ, by fitting eq. (7), to be 2×10^4 m^{-1}. While this value is at the lower end of those reported in the literature, it remains within the same order of magnitude. This difference may be attributed to the larger size of *H. lacustris* cells, which are less densely packed, allowing deeper light penetration within the biofilm, consistent with observations by Kiperstok et al. [66];

- Carbon-specific biomass density (ρ_C): Mature biofilms exhibit a biofilm thickness (h) of approximately 700–900 μm for a biomass areal density of 24–31 g_C m^{-2} [77], implying a carbon-specific biomass density of 35×10^3 g_C m^{-3} ($\rho_C = X/h$). Other researchers [76,78] estimated their biofilm densities to be around 60–80 $\times 10^3$ g_C m^{-3} explaining their higher extinction coefficient and giving merit to the aforementioned hypothesis that *H. lacustris* are less densely packed;
- Nitrogen Half-Saturation Constant (K_S): Half-saturation concentrations for nitrate uptake among freshwater microalgae, typically fall in the range of 0.3–3 μM of N. Therefore, K_S was fixed to an average value of 0.7 μM of N or 0.01 g_N m^{-3} [79,80];
- Respiration Rate (R): Set to 10 % of μ_{max} [1,81]. Other approaches have modeled respiration by incorporating the cost of biosynthesis (proportional to the substrate uptake rate, r_S) [42,69,82]. However, it is widely reported that respiration increases during nitrogen starvation in *H. lacustris* [83–85], which would contradict a model where respiration is directly tied to substrate uptake.

The measured outputs for the model include the biomass areal density in the biofilm, as well as the intracellular nitrogen, chlorophyll, and astaxanthin quotas, which represent four of the six state variables from Table 2. Standard deviations (σ) were assigned to each output to account for experimental errors in biomass quantification, pigment extraction, and elemental analysis [13]. These deviations are depicted as error bars in the plots in the Supplementary Materials. Given the variability of these errors across the dataset, representative standard deviations were established: σ_X at 1 g_C m^{-2}, σ_q at 0.005 g_N g_C^{-1} and both σ_θ and σ_w at 0.002 g_N g_C^{-1}.

3.5.2. Model validation

Model validation was performed using independent datasets not employed in the parameter estimation (Table 1). Error bars in the plots represent the measured experimental standard deviations of each variable. For the reversion dataset with single measurements, individual data points are presented without error bars.

To integrate parameter uncertainties into the model predictions, a 95 % confidence envelope was generated around the nominal model trajectory. This was achieved by sampling parameter sets within their respective 95 % confidence intervals obtained from the MLE. The model was simulated for each parameter set, and the confidence envelope was constructed by identifying the maximum and minimum values across all simulations at each time point.

3.6. Optimization

In rotating systems, continuous operation implies that biofilms are harvested from the carrier while the remaining colonies on the substrate serve as inoculum for the next growth cycle [78,86,87].

As a case study, we develop an optimization strategy to maximize astaxanthin density, $P_w(t)$ [g_{Astx} m^{-2}], defined as the product of biomass density, $X(t)$, and astaxanthin quota, $w(t)$. The optimization variables consist of the light intensity time profile ($0 \leq I_0(t) \leq 2000$ μmol m^{-2} s^{-1}), as well as the harvesting times, t_f. We assume that after harvesting, a new cycle is initiated with an initial condition of 1.25 g_C m^{-2} (equivalent to 35 μm of residual biomass on the carrier), maintaining the physiological conditions of the previously harvested biomass, in terms of q, w and θ. Nutrients are reintroduced to the system immediately after harvesting at an initial nutrient concentration of 100 g_N m^{-3}, replicating the conditions employed in the experimental campaign. It is assumed that no planktonic culture is added to the system.

4. Results

4.1. Parameter estimation and model validation

The model describes all biofilm traits, the key stages of the *H. lacustris* life cycle, overall biofilm growth, and reversibility from the red to the green stages (Figs. 2 and 3). Values of the estimated parameters and their 95 % confidence intervals are reported in Table 4 (variance and correlation matrices are available in Table S1 and S2). All parameters were identifiable with statistical significance and closely matched biological features found in the literature for both experimental and modeling approaches on *H. lacustris* and freshwater phytoplankton.

The model showed good capability in simulating the initial adhesion of cells (from Day 0 up to Day 2). During the low light (LL) green stage, at light intensities of 50 and 200 μmol m^{-2} s^{-1}, the model accurately predicts the light-limited condition and the observed plateau in biomass density (Figs. 2A and 3A). As light intensity increases, the model describes the rapid increase in biomass growth in both green and red high-light (HL) stages, followed by a slowdown in growth, as nutrient availability decreases.

Chlorophyll and astaxanthin quotas respond significantly to changes in light intensity and nitrogen availability. Under nitrogen-replete conditions, chlorophyll quota undergoes photo acclimation during both the LL and HL stages (Figs. 2C and 3C). There is an initial reduction in chlorophyll content at 200 μmol m^{-2} s^{-1} compared to 50 μmol m^{-2} s^{-1}, followed by a recovery between Days 4 and 7 as biofilm thickness increases and light is attenuated. A similar trend was observed in the HL stage, where increased light intensity induces a decrease in chlorophyll quota (Fig. 2C). These chlorophyll dynamics directly influenced astaxanthin levels, which follow similar trends with an increased accumulation of astaxanthin under higher PPFD, even when nutrients are available (Fig. 2D).

The intracellular nitrogen quota is also well described by the model, particularly once the substrate is depleted from the reactor. Nitrogen was removed on Day 7 for nitrogen-depleted conditions, or fully consumed between Days 12 and 15 for nitrogen-repleted conditions (data not shown). The model predicts this nutrient consumption and the resultant physiological adjustments within the biofilms. As nitrogen is depleted, there is a concurrent decrease in intracellular nitrogen quota (Figs. 2B and 3B) and chlorophyll quota (Figs. 2C and 3C), alongside an accumulation of astaxanthin within the cells, a stress response that is acting synergistically with the higher light intensity (Figs. 2D and 3D).

In the final set of experiments (Fig. 3), nitrogen is reintroduced into the medium at Day 14 to assess the reversibility of *H. lacustris* from the red to the green stage. Experimentally, with the substrate reintroduction, biomass growth restarts, the intracellular nitrogen quota is quickly restored and so is the chlorophyll quota to a level that is comparable to that observed for biofilms photoacclimated at 400 μmol m^{-2} s^{-1} (Fig. 3B and C). This restoration is followed by the degradation of astaxanthin at a slower rate (Fig. 3D).

However, across all experimental conditions, irrespective of light intensities and nitrogen levels (Figs. 2A, 3A and Supplementary Materials), the model consistently underestimates biomass densities exceeding 15 g_C m^{-2} when compared to the observed experimental data.

4.2. Biofilm gradients

Measuring growth rate, chlorophyll, and astaxanthin gradients

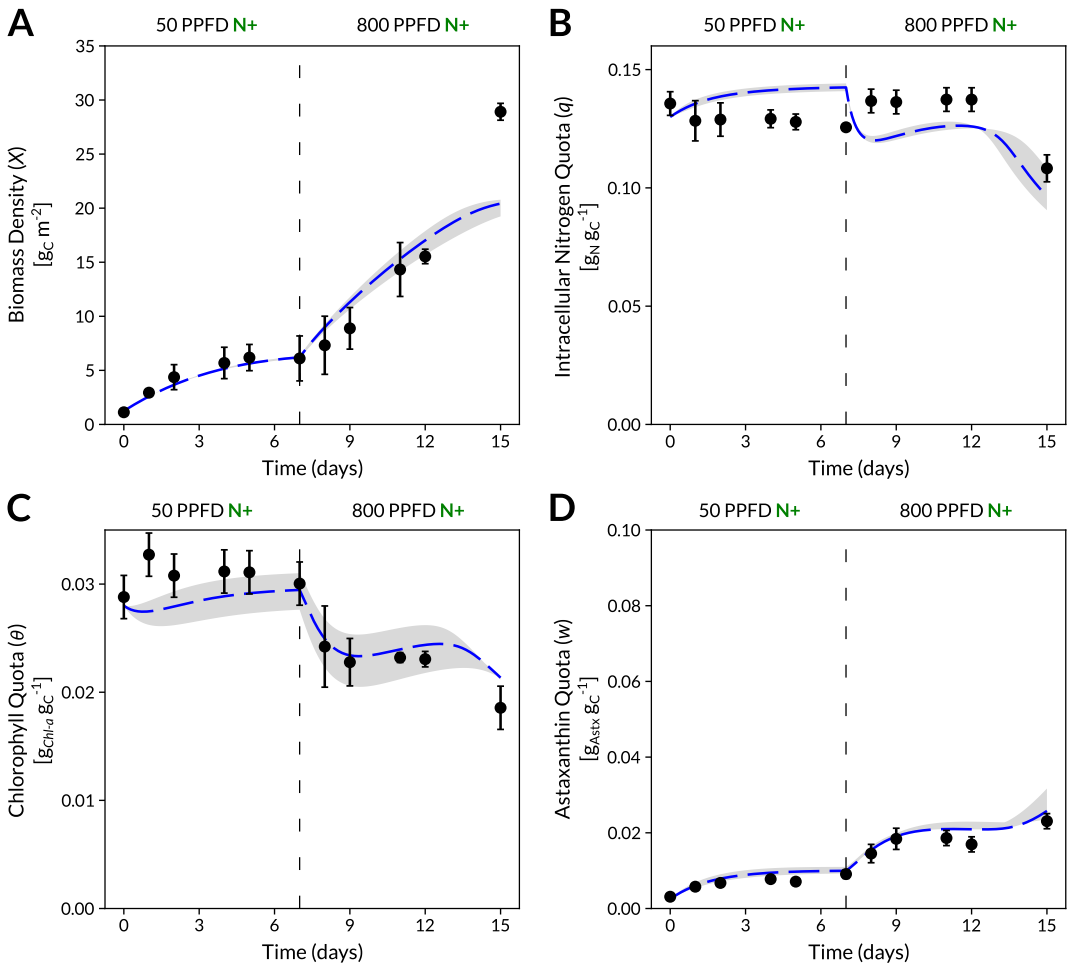


Fig. 2. Model prediction (dashed lines) compared with experimental data for a green stage only scenario (filled markers with error bars, number of replicates, $n = 2$). Growth conditions are as follows: from Day 0 to Day 7, the green stage at 50 μmol m^{-2} s^{-1} under nitrogen-replete conditions (N+); from Day 8 to Day 15, nutrients are reintroduced to the medium (N+), and light is increased to 800 μmol m^{-2} s^{-1}. Each panel depicts a biofilm trait: (A) biomass density [g_C m^{-2}], (B) intracellular nitrogen quota [g_N g_C^{-1}], (C) chlorophyll quota [$g_{Chl\text{-}a}$ g_C^{-1}], and (D) astaxanthin quota [g_{Astx} g_C^{-1}]. The 95 % confidence interval is represented by the grey area enveloping the model prediction. (For interpretation of the references to colour in this figure legend, the reader is referred to the web version of this article.)

experimentally in a biofilm remains challenging. However, by modeling light attenuation over depth, valuable insights into these gradients can be obtained at specific time points, including their time evolution. This approach enables the prediction of growth rate and the distribution of astaxanthin and chlorophyll across the biofilm in order to better understand the physiological processes and dynamics at play that would otherwise be inaccessible. These insights are particularly important for optimizing cell physiology during harvesting and preparing for subsequent growth cycles.

Macroscopic and microscopic images of the biofilms are reported in Fig. 4A and B where a gradient over depth can be seen. The distribution of astaxanthin, chlorophyll and growth rate across biofilm depth is depicted in Fig. 4C and D respectively (Day 14 represent astaxanthin-dominated biofilm and Day 21 reflects the biofilms after nutrient reintroduction leading to reversion). On Day 14, astaxanthin levels ranged between 3.5 % and 5.0 % of dry weight (DW%), while chlorophyll-*a* levels range between 0.4 and 0.7 DW%. Biofilm stratification is not pronounced, with astaxanthin content above 3.5 DW% and chlorophyll below 0.7 DW% across the biofilm.

Conversely, at Day 21, the reverted biofilm shows a clear stratification with cells in different metabolic states (Fig. 4B and C). The upper 100 μm of the biofilm contains cells in an intermediate state transitioning from red to green stage, with astaxanthin between 1 and 2 DW % and chlorophyll-*a* at 0.9–1.2 DW%. Deep within the biofilm, the population is dominated by green-stage cells, exhibiting lower astaxanthin content around 0.6 DW% and higher chlorophyll-*a* content around 1.3 DW%.

Both biofilm profiles on Day 14 and Day 21 depict a classical growth response over depth (Fig. 4D). Photoinhibition is observed at the surface of the biofilms, with optimal growth occurring at 20 μm below the surface. Beyond this depth, light limitation becomes more pronounced, and respiration dominates over growth after the light intensity falls below the compensation point around 70–140 μm.

The observed differences in growth rates before and after reversion are driven by the intracellular nitrogen quota. This synergetic interaction leads to a net negative growth rate by Day 14 (as shown in Fig. 4D, ($\bar{\mu} = -0.05$ d^{-1}), contrasting with the positive net growth rate noted at the end of the reversion phase ($\bar{\mu} = 0.04$ d^{-1}). Despite the presence of high chlorophyll levels (close to θ_{max}), most of the biofilm remains metabolically inactive. Biofilm development primarily occurs through the accumulation of new cells within the photoactive layer near the surface, while deeper layers maintain a state of relative metabolic dormancy.

4.3. Optimization strategy

One of the model's key applications is the optimization of astaxanthin production in biofilm technology. The harvesting frequency and light conditions resulting from the optimization analysis for maximizing astaxanthin density (P_w) are shown in Fig. 5.

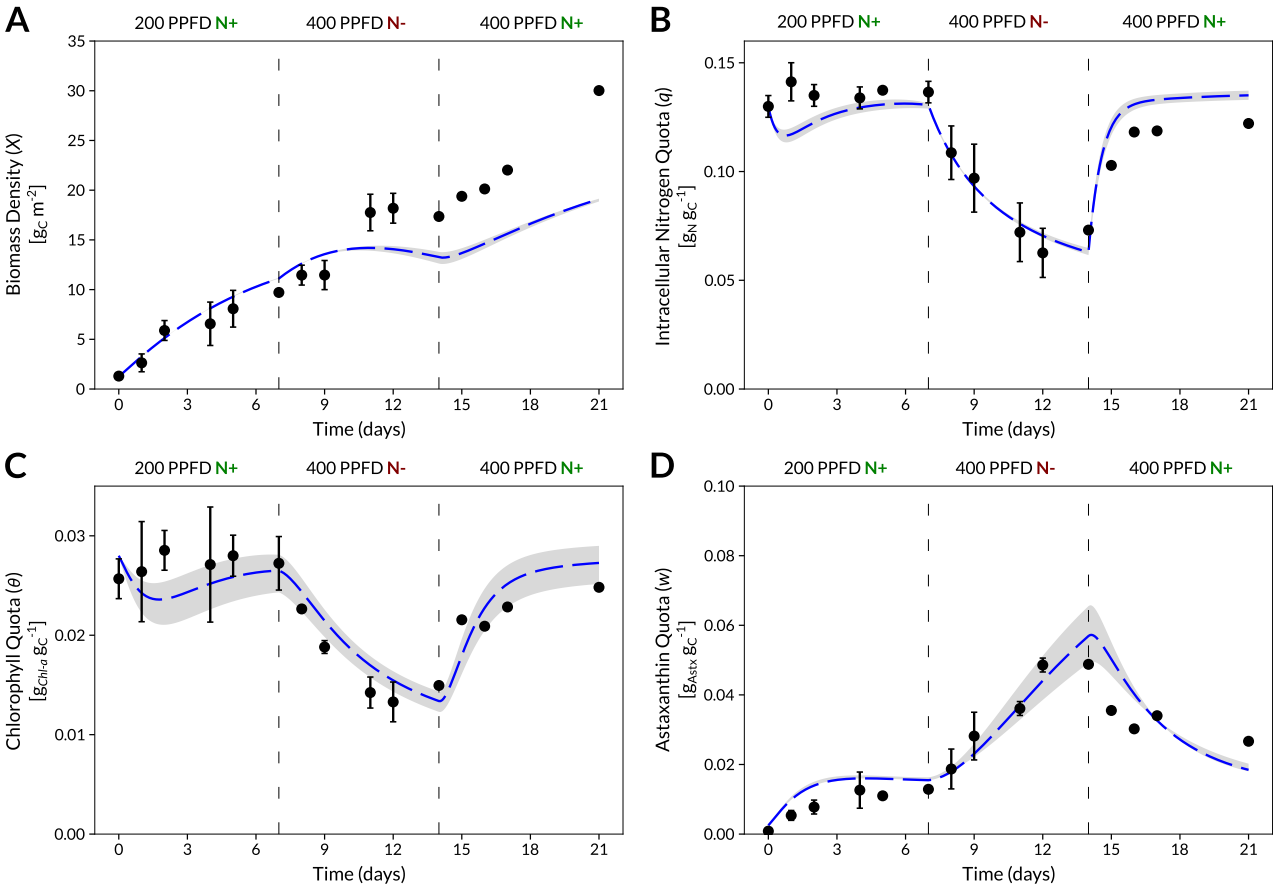


Fig. 3. Model prediction (dashed lines) compared with experimental data for a reversion scenario – green to red back to green (filled markers with error bars, number of replicates, $n = 3$). Growth conditions are as follows: from Day 0 to Day 7, the green stage at 200 μmol m^{-2} s^{-1} under nitrogen-replete conditions (N+); from Day 8 to Day 14, the red stage at 400 μmol m^{-2} s^{-1}under nitrogen-deplete conditions (N-); from Day 15 to Day 21, nutrients are reintroduced to the medium (N+), light is maintained at 400 μmol m^{-2} s^{-1}, and the biofilm reverts from the red to the green stage ($n = 1$). Each panel depicts a biofilm trait: (A) biomass density [g_C m^{-2}], (B) intracellular nitrogen quota [g_N g_C^{-1}], (C) chlorophyll quota [$g_{Chl\text{-}a}$ g_C^{-1}], and (D) astaxanthin quota [g_{Astx} g_C^{-1}]. The 95 % confidence interval is represented by the grey area enveloping the model prediction. (For interpretation of the references to colour in this figure legend, the reader is referred to the web version of this article.)

The first production cycle starts on Day 0, under the same conditions as the experimental design used for parameter estimation (Table 2). The strategy elaborated by the optimization algorithm was to gradually increase light exposure from ~515 μmol m^{-2} s^{-1} to the maximum of 2000 μmol m^{-2} s^{-1} during the first 81 h, then the strategy consisted of maintaining it at its maximal value until the biofilm is harvested.

Nutrients are depleted by Day 9, and biofilm thickness of 396 μm is harvested by Day 16, leaving 35 μm of biomass on the cotton carrier. This residual biomass is crucial for restarting the next cycle; it retains an intracellular nitrogen quota of 0.058 g_N g_C^{-1}, a chlorophyll quota of 0.012 $g_{Chl\text{-}a}$ g_C^{-1} (content of ~0.621 DW%), and an astaxanthin quota of 0.070 g_{Astx} g_C^{-1} (~ 3.63 DW%). Due to stratification, the average astaxanthin content of the harvested biomass is higher (while average chlorophyll content is lower) than that of the cells at the biofilm's bottom layer, a difference evident at the end of one cycle and the beginning of the next (Fig. 5E).

The next cycle begins immediately after harvesting, with nutrients reintroduced into the system. This cycle differs from the first, as the cells left on the cotton carrier are under stress and must undergo reversion. The light intensity is again increased gradually, from a slightly lower light intensity ~495 μmol m^{-2} s^{-1} and over a longer period of 94 h. This gradual increase helps maintaining the average light level near the optimal intensity within the biofilm (Fig. 5C), supporting biomass growth before imposing another stress. The intensity of 2000 μmol m^{-2} s^{-1} is then applied until the biofilm is harvested. By Day 9, nutrients are again depleted, and after 16.5 days, 390 μm of biofilm is harvested. A third cycle is repeated with similar optimized light conditions, finally achieving a steady-state. The steady-state cycle is shown as the fourth cycle in Fig. 5: 390 μm of biofilm is harvested, retaining 0.058 g_N g_C^{-1}, a chlorophyll quota of 0.012 $g_{Chl\text{-}a}$ g_C^{-1} (~ 0.622 DW%), and an astaxanthin quota of 0.07 g_{Astx} g_C^{-1} (~ 3.65 DW%).

5. Discussion

5.1. Astaxanthin models

The proposed dynamic model is the first to describe the production of high-value compounds (i.e. astaxanthin) using rotating microalgae biofilms. It captures the complex dynamics of biofilm growth and composition, demonstrating high accuracy in predicting physiological responses to varying light intensities, nitrogen availability and cultivation stages.

Existing models describing astaxanthin production in *H. lacustris* are mostly limited to planktonic cultures. The works of Del Río et al. [33,94] and García-Malea et al. [34,95,96] assessed a one-stage production model in which growth and astaxanthin accumulation are functions of light, accounting for photolimitation and photoinhibition, as well as specific nitrate input. Astaxanthin production is modeled using the Luedeking-Piret equation, wherein the growth-independent term of the specific accumulation rate of astaxanthin depends on the average light intensity and is modulated by a substrate limitation-inhibition function. These models are simple and accurately track experimental data even in

Table 4
Model parameters, including fixed variables and estimated parameters using maximum likelihood estimation (MLE) and respective standard deviation (std) and 95 % confidence intervals (CI).

Parameter	Value ± std	95 % CI	Unit	Equation	Literature
k	0.17	–	d^{-1}	Fixed	–
ρ_C	35×10^4	–	$g_C\ m^{-3}$	Fixed	60 to 80 $\times 10^4$
ϵ	2×10^4	–	m^{-1}	Fixed	1.8 to 11.6 $\times 10^4$
$\delta_\theta = \mu_{max}$	0.982 ± 0.024	(0.936, 1.029)	d^{-1}	Estimated	0.65 to 1.3
R	10 % μ_{max}	–	d^{-1}	Fixed	10 % μ_{max}
α	0.021 ± 0.002	(0.017, 0.024)	d^{-1}	$\alpha^{Chl} \times \mu_{max}$	0.007 to 0.13
α^{Chl}	0.662 ± 0.055	(0.553, 0.771)	d^{-1}	Estimated	0.5 to 1.5
I_{opt}	94 ± 9	(77, 111)	$\mu mol\ m^{-2}\ s^{-1}$	Estimated	50 to 177
q_{max}	0.149 ± 0.001	(0.147, 0.151)	$g_N\ g_C^{-1}$	Estimated	0.14 to 0.35
q_{min}	0.051 ± 0.002	(0.047, 0.055)	$g_N\ g_C^{-1}$	Estimated	0.023 to 0.058
K_S	0.01	–	$g_N\ m^{-3}$	Fixed	0.004 to 0.04
$r_{S_{max}}$	0.146 ± 0.004	(0.139, 0.154)	$g_N\ g_C^{-1}\ d^{-1}$	$\mu_{max} \times q_{max}$	0.003 to 0.147
γ_m	0.211 ± 0.004	(0.204, 0.218)	$g_{Chl\text{-}a}\ g_N^{-1}$	Estimated	0.11 to 0.35
K_I	251 ± 65	(123, 380)	$\mu mol\ m^{-2}\ s^{-1}$	Estimated	> 175
$\widetilde{w}$	46.9 ± 2.7	(41.6, 52.2)	$g_{Astx}\ g_C^{-1}$	Estimated	–
η	0.0060 ± 0.0001	(0.0058, 0.0062)	$g_{Chl\text{-}a}\ g_C^{-1}$	Estimated	–
δ_w	0.367 ± 0.032	(0.304, 0.430)	d^{-1}	Estimated	–
θ_{max}	1.42 ± 0.03	(1.36, 1.47)	DW%[a]	$\gamma_m \times q_{max}$	1.0 to 1.5 %
θ_{min}	0.06 ± 0.02	(0.03, 0.09)	DW%[a]	[b]	< 0.2 %
w_{max}	5.38 ± 0.033	(4.74, 6.03)	DW%[a]	$\widetilde{w}\frac{\eta}{e}$	5 %

μ_{max}: [88,89]; α^{Chl}: [56]; α, r_{Smax}: [80]; q_{max}, q_{min} : [80,90,91]; I_{opt}, K_I, w_{max} : [6,30]; γ_m: [42,64,91]; $\theta_{max}, \theta_{min}$: [92].

[a] Literature values usually are reported in terms of pigment content as a percentage of dry weight [DW%]. To convert quota [$g\ g_C^{-1}$] to DW%, it is assumed that during the green and red stages, elemental carbon represents 45–52 DW% [13,93];

[b] θ_{min} can be found using Eq. (12) and Eq. (13) at steady state, for a single cell at q_{min} and at the surface of the biofilm exposed to a light intensity of 2000 $\mu mol\ m^{-2}\ s^{-1}$.

large outdoor systems, but estimated parameters, such as maximum growth rates, showed significant variability even for the same species and reactor, ranging from 0.64 to 2.64 d^{-1}. Zhang et al. [37] presented the first and sole model describing astaxanthin and biomass production in an attached cultivation system, assessing the effects of light attenuation, temperature, and nitrogen-depletion conditions. The maximum growth rate reported aligns with our findings (0.783 d^{-1} at 25 °C). Their approach uses a normalized nitrogen quota, expressed on a dry weight basis, to address the lack of direct measurements, with a minimum quota significantly higher than our findings (0.165 gN/gDW ~ 0.08 $g_N\ g_C^{-1}$). Their model suggested that nitrogen deficiency initially stimulates biomass growth, contrasting with our standard Droop approach. Additionally, Zhang et al. [37] proposed a maximum astaxanthin content of 7 DW%, which is higher than both the typical values reported in the literature and our estimation of 5.4 DW%.

The main strength of the model developed in this study, compared to the previously described models, is that astaxanthin is for the first time modeled as a function of chlorophyll dynamics, based on the well-established understanding of photoacclimation dynamics. This methodology is based on physiological mechanisms such as chlorophyll synthesis, sharing also dependencies on light and intracellular nitrogen quota.

5.1.1. A new modeling approach to predict astaxanthin dynamics

The main novelty in our model lies in establishing a correlation between chlorophyll and astaxanthin cell dynamics, ensuring that dependencies on light and nitrogen simultaneously affect both state variables, reducing the number of parameters and conserving biological features. It posits that astaxanthin dynamics are guided by those of chlorophyll at an equilibrium, determined by the acclimation rates δ_θ and δ_w. The chlorophyll rate δ_θ was fixed equal to μ_{max}, while the astaxanthin rate δ_w was lower, suggesting that chlorophyll degradation occurs faster than astaxanthin accumulation. This aligns with the sequence of metabolic events observed in response to nitrogen starvation and high light: inhibition of chlorophyll biosynthesis occurs alongside a decline in photosynthetic activity and activation of the xanthophyll cycle [85]. Starch accumulates and is later degraded in favor of fatty acid synthesis [97,98]. Carotenogenesis is triggered, and β-carotene is exported from the chloroplast to the endoplasmic reticulum, where it is converted into astaxanthin and esterified with lipid droplets [99]. These mechanisms lead to the formation of mature haematocysts, characterized by a significant decline in chlorophyll and metabolic activity, with photoprotection primarily provided by astaxanthin optic shielding [100].

The activation of photoprotective mechanisms and the disruption of the photosynthetic apparatus limit cells ability to efficiently utilize light for astaxanthin synthesis. In our model, the proposed chlorophyll-astaxanthin equation identifies an optimal chlorophyll quota that maximizes astaxanthin production, Eq. (15). Beyond this optimal point, any further reduction in chlorophyll results in a decline in astaxanthin levels (Fig. 1D). This phenomenon has also been observed by Samhat et al. [101,102], who correlated astaxanthin productivity with the mean light absorption rate of *H. lacustris* biomass. Notably, our equation aligns with their experimental findings ($R^2 = 0.90$, Fig. S10).

5.1.2. Model improvements

The model matches the observed data at all life cycle stages, highlighting its ability to simulate dynamic environmental changes and their impact on biofilm physiology. However, some discrepancies remain, particularly in biomass predictions. The model underestimates biomass densities above 20 $g_C\ m^{-2}$ for both nitrogen-replete and nitrogen-deplete conditions, predicting a much slower growth compared to experimental observations (Fig. 2A and Fig. 3A, calibration experimental datasets in Supplementary Materials, Fig. S2–7). This inaccuracy can be predominantly explained by the life cycle of *H. lacustris*. In the red stage, while cell division stops, biomass continues to increase due to the accumulation of starch and lipids, leading to a higher carbon-per-cell ratio [6,103]. This aspect, not accounted for in the current model, could be improved by incorporating cell cycle dynamics, division, and size variation [104]. Additionally, measurements of the harvested

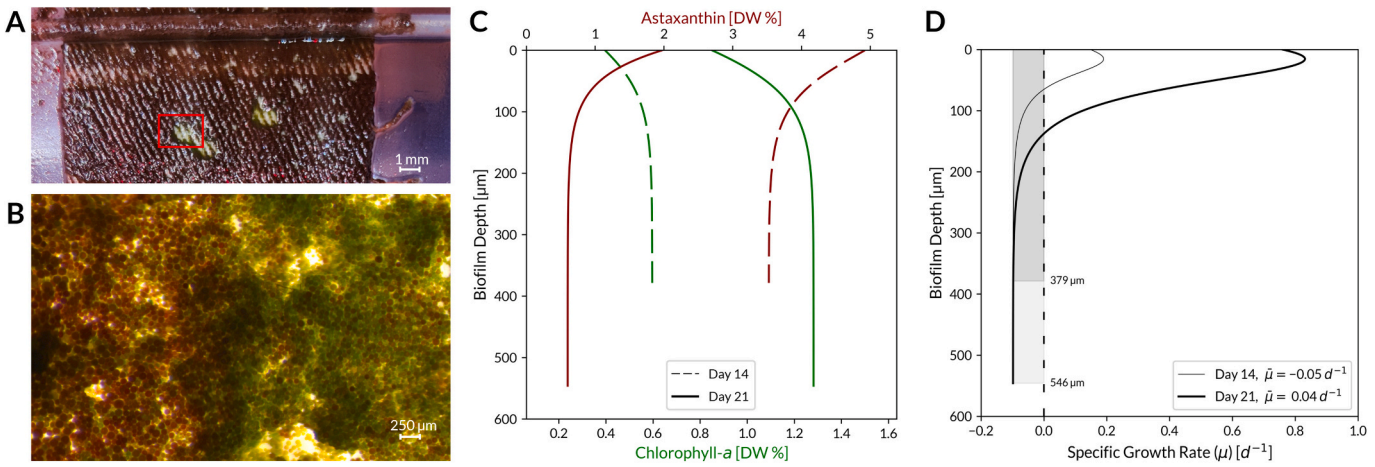


Fig. 4. Gradients of astaxanthin, chlorophyll and growth rate over biofilm depth. (A) Macroscopic view of a red-stage biofilm *Haematococcus lacustris* biofilm on a cotton carrier. A region of the biofilm was manually removed (highlighted area) to expose the underlying layer of green cells on the cotton substrate. (B) Stereoscopic microscope image of the region outlined in (A), showing the biofilm stratification. On the left, the biofilm remains intact, displaying predominantly large red haematocycsts (astaxanthin-rich). On the right, the exposed area reveals the bottom layer of the biofilm consisting of a mixture of green and red cells of varying sizes. (C) Profile of astaxanthin and chlorophyll-*a* content (DW%) across the biofilm depth for the experimental campaign of biofilm reversion. Dashes lines represent the end of the red-stage in an astaxanthin-dominant biofilm (Day 14). Solid lines correspond to Day 21, the end of the experiment after nutrient reintroduction leading to reversion. (D) Specific growth rate at Day 14 and Day 21: the average net growth rate over the biofilm cross-section is $\bar{\mu} = -0.05\ d^{-1}$ and $\bar{\mu} = 0.04\ d^{-1}$ at Day 14 and Day 21, respectively. (For interpretation of the references to colour in this figure legend, the reader is referred to the web version of this article.)

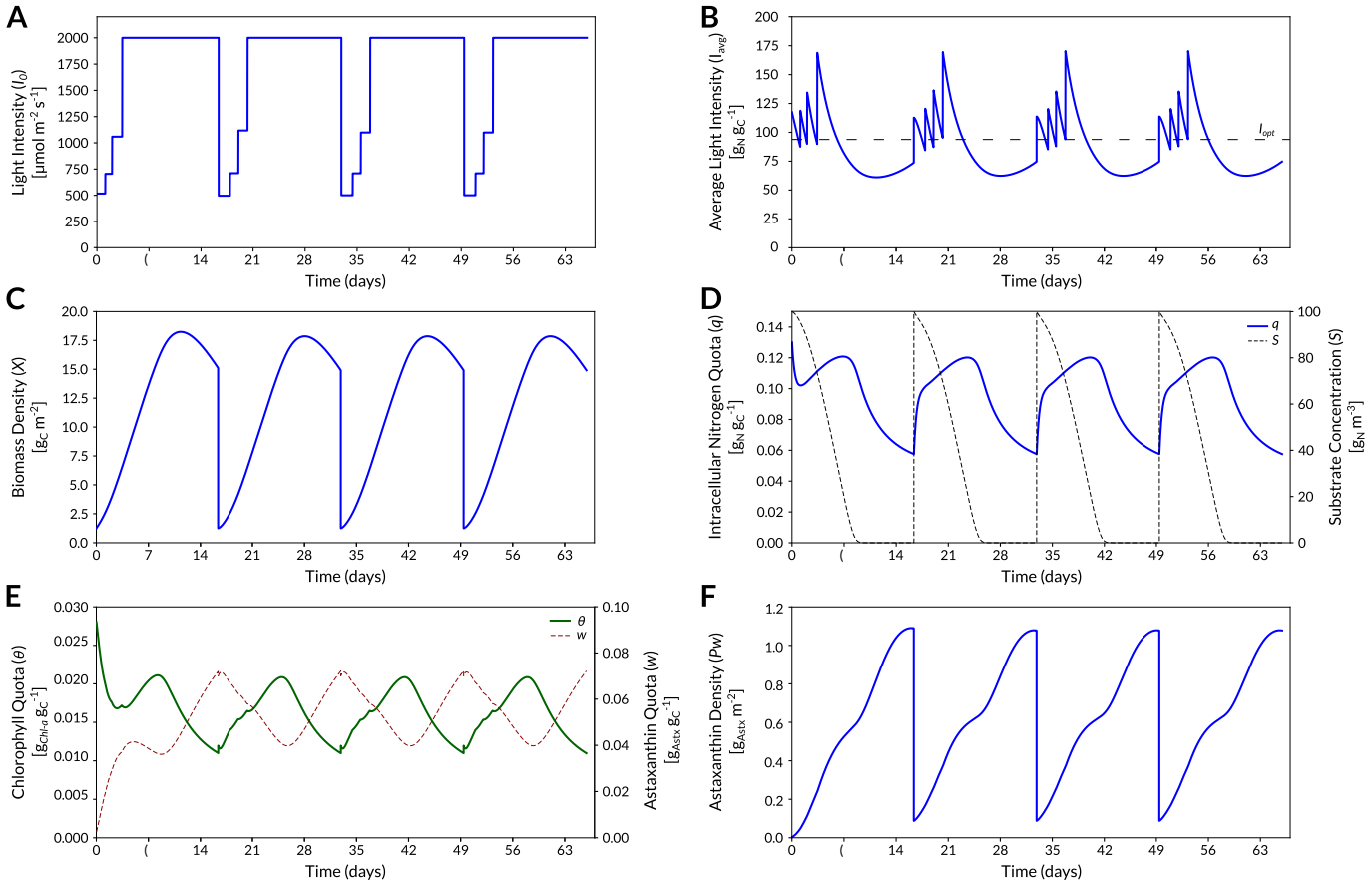


Fig. 5. Evolution of the biofilm traits over multiple production cycles (66 days): a first cycle to start the processes (16.5 days), followed by two repeated harvest and re-growth cycles until a steady state is achieved. (A) Optimized light intensity profile (I_0) [µmol m^{-2} s^{-1}]; (B) Average light intensity over the biofilm depth (I_{avg}) [µmol m^{-2} s^{-1}]; (C) Biomass density (X) [g_C m^{-2}]; (D) Intracellular nitrogen quota (q) [g_N g_C^{-1}] (solid line) and substrate concentration (S) [g_N m^{-3}] (dashed line); (E) Average chlorophyll quota (θ) [$g_{Chl\text{-}a}$ g_C^{-1}] (solid line) and average astaxanthin quota (w) [g_{Astx} g_C^{-1}] (dashed line); (F) Astaxanthin density, P_w [g_{Astx} m^{-2}] maximized in the objective function.

biofilm's dry weight and elemental composition include not only cells but also extracellular polymeric substances (EPS) and other cell structures that are excreted after cell division (e.g., theca) [105,106]. All these components were excluded from the model due to a lack of direct measurement, but their inclusion could help better capture biofilm growth dynamics in future work.

To further enhance the model, a more detailed biofilm profile could be developed using a spatially distributed model that incorporates EPS and additional compounds. Describing substrate diffusion within the biofilm and dissolved inorganic carbon gradients [25,107] would enable the computation of nutrient requirements to support growth and selectively target astaxanthin production at different biofilm depths. Oxygen is another key compound, as its accumulation can significantly inhibit growth in both planktonic cultures [108,109] and photosynthetic biofilms [29,110]. On the other hand, oxygen may enhance astaxanthin accumulation, as the overproduction of reactive oxygen species (ROS) in the cells acts as an additional stressor [111,112]. Finally, incorporating transition state models, with accurate light-harvesting parameters and dynamically implementing dark-light cycles would be beneficial [91,113]. However, more research is needed to determine the optimal harvesting light parameters for *H. lacustris*. Limited studies are available on the photosynthetic-irradiance response for this species [88,114], as well as on measurements of quantum yield and photosynthetic efficiency [85,100,115]. These studies highlight the complexity of the *H. lacustris* life cycle and the challenge of accurately and precisely determining these parameters experimentally.

5.2. Reversion dynamics and optimization

A two-stage process is traditionally employed for producing astaxanthin in *H. lacustris*, while a one-stage process would greatly reduce operational costs and complexity [33,96,102]. In planktonic systems, a two-stage process can jeopardize productivity due to unsynchronized and heterogeneous cells, which have lower astaxanthin content and are harder to settle down and harvest [116]. In microalgae biofilms, where biomass is physically separated from the medium, a two-stage process with its physiological advantages can be significantly simplified by adopting the operational advantages of a one-stage process [12,13]. This can be accomplished through the continuous operation of a rotating system, allowing for repeated harvest and regrowth cycles.

In *H. lacustris* biofilms, the ideal scenario is for astaxanthin to accumulate in the top biofilm layer leaving the cells in the bottom layer in the green stage, ready for the next cycle. This concept, proposed and observed by Kiperstok et al. [12] and Zhang et al. [16], is illustrated in Fig. 4A and B. However, mechanically harvesting only the astaxanthin-rich layer is challenging, as it represents only a small percentage of the biofilm. In a more realistic scenario, where all biofilm layers are harvested, the remaining cells in tight contact with the carrier must be ready for the next cycle [86]. For cells to revert from the red stage, they must switch back to the metabolically active green stage before growth can resume. This biological reversion needs to be validated to explore the development of optimization strategies for continuous production.

5.2.1. Life cycle reversion: from red to green stage

In this study, we demonstrated, both experimentally and mathematically, that the reversion from the red to green stage in *H. lacustris* biofilms is possible. The reversion experiment was only performed once, as proof of concept, to verify and validate the model capabilities in predicting the stage reversion in *H. lacustris*. Therefore, further experiments will be necessary to strengthen the statistical relevance of these data. During reversion, chlorophyll amounts were restored more rapidly, while astaxanthin degraded slowly as cells recovered and shifted their metabolic activity back to growth (Fig. 3). These results are consistent with the observations of Samhat et al. [102], who reverted an *H. lacustris* culture in a continuous photobioreactor over 15 days. By day 10, chlorophyll levels had nearly returned to their previous maximum, while astaxanthin remained at half of its maximum content.

Experimentally, the intracellular nitrogen quota in the biofilm does not fully revert (Fig. 3B), which may be attributed to the complex metabolic reorganization the cells undergo during the recovery phase. It is known that recovery from starvation requires a reorganization of the proteome (e.g., de novo synthesis of transporters and photosystems), structural and compositional adjustments of lipids in thylakoid membranes, and relaxation of photoprotective mechanisms [117]. Other researchers [118,119] observed that, during reversion, the recovered green cells retain higher levels of non-photochemical quenching (NPQ) than the initial ones. This serves as a mechanism to protect the new green cells from light fluctuations, optimizing light-use efficiency. This phenomenon is similar to the priming effect described by Morgado et al. [13] in *H. lacustris* biofilms, where cells primed to mild-stress conditions could withstand higher stress and better survive under unfavorable conditions. Similarly, cells reverting from red to green may retain stress-related characteristics (mid-levels of astaxanthin content) for a period, as they were metabolically pre-trained to withstand higher excitation pressure.

Partial reversion could also be explained by the loss of activity deep into the biofilm. Based on the growth rate profiles over depth (Fig. 4), corroborated with experimental observation reported in other studies [120,121], photo-limitation and dark respiration can lead to a negative net growth rate in the biofilm. Polizzi et al. [29], who modeled 2D photosynthetic biofilms, also described that most of the deep layers are represented as an inert fraction, with only the outer microalgae remaining active and contributing to the functional fraction of the biofilm. This stratification could confine reversion to the top layers, leading to discrepancies in the intracellular quotas of nitrogen and pigments between the model and experimental observations.

5.2.2. Optimization strategy and future applications

The model successfully predicted reversion dynamics and consequent physiological responses (growth and intracellular quotas of nitrogen and pigments) without prior training on the reversibility conditions (Fig. 3). This achievement led to the development of an optimization strategy for maximizing astaxanthin density through repeated harvest and regrowth cycles (Fig. 5).

The proposed strategy involves adjusting both light conditions and harvesting frequency. Maximizing astaxanthin density requires balancing periods of active growth, where average light within the biofilm is near optimal while nutrients are still available, with periods of stress characterized by maximum light intensity and nutrient starvation [122]. While these stress conditions trigger astaxanthin synthesis, they also lead to biomass loss due to a net negative growth rate, a pattern observed in all harvest regrowth cycles (Fig. 5A). Moreover, the optimization indicates that once cells are stressed, adjustment in light intensity and duration are necessary to revert the cells to an active state under nutrient-replete conditions.

Therefore, assessing full-cycle productivities is crucial for astaxanthin production accounting for the idle time between the two stages. However, reported astaxanthin productivities in the literature often consider only the red stage, overlooking the green stage's contribution and the associated operational downtime between growth and stress stages. This omission can lead to inflated productivity figures, as seen in other studies [12–14,16]. By accounting for the entire growth-stress-reversion cycle, a more comprehensive and realistic assessment of astaxanthin productivity is provided.

The optimization yielded a full-cycle astaxanthin productivity (accounting for both green and red stages) of 0.065 $g_{Astx}\ m^{-2}\ d^{-1}$, marginally surpassing the best scenario identified during model calibration (0.062 $g_{Astx}\ m^{-2}\ d^{-1}$; Fig. S8). These findings suggest that further improvements in astaxanthin productivity will likely result from integrated optimization strategies that extend beyond light manipulation. Indeed, because nitrogen was not controlled in the current optimization and became depleted by day 9 in all harvest regrowth cycles, it

emerged as the limiting factor, preventing additional increases in light intensity from enhancing astaxanthin accumulation.

Thus, nutrient management strategies such as fed-batch approaches that maintain optimal chlorophyll levels should be investigated, similar to the one-stage production methods demonstrated in the works of Samhat et al. [101,102], Del Río et al. [94], and García-Malea et al. [96]. Furthermore, exploring variables such as harvest percentage and alternative harvesting patterns [29,123], as well as implementing automated and precise harvesting mechanisms, could lead to strategies that prevent negative growth rates in deeper biofilm layers and improve overall productivity.

Finally, coupling the proposed model with technologies capable of providing real-time data on biofilm traits without disrupting the biofilm structure [77] could empower the development of advanced monitoring and control strategies for biofilm-based astaxanthin production processes [124]. This integration would in turn enhance scalability and cost-efficiency, paving the way for the industrial-scale adoption of biofilm technology.

6. Conclusions

A dynamic model was developed to simulate the growth and astaxanthin production in *H. lacustris* biofilms. The model features a novel approach to estimating astaxanthin dynamics based on those of chlorophyll, providing a comprehensive model that describes average growth rate, light attenuation, intracellular nitrogen, chlorophyll and astaxanthin quotas.

The model's predictions closely align with observed data across various life cycle stages in all validation datasets, demonstrating its ability to effectively simulate dynamic environmental changes and their impact on biofilm physiology. We used the model to estimate gradients across the biofilm, in particular growth and pigments distribution, based on which we could confirm the possibility of dynamically altering the life cycle of *H. lacustris* within a biofilm, transitioning from green to red stages and vice versa.

Remarkably, the model predicted the trends of these dynamic physiological responses without prior training on reversion data. This capability allowed us to develop an optimization strategy to maximize astaxanthin density, suggesting that continuous astaxanthin production is feasible through repeated harvest and regrowth cycles by optimizing light intensity and harvesting frequency, which is essential for scaling-up this process at the industrial level.

Future efforts will focus on validating the optimization strategy and integrating the model with online monitoring tools. Also, more combinations of environmental conditions should be tested to make the model more robust under real process conditions where several parameters can change in parallel. These steps will further advance the development of continuous production systems, facilitating the industrial-scale implementation of biofilm technology for high-value compounds.

CRediT authorship contribution statement

David Morgado: Writing – review & editing, Writing – original draft, Validation, Software, Formal analysis, Data curation, Conceptualization. **Andrea Fanesi:** Writing – review & editing, Writing – original draft, Validation, Supervision, Investigation, Formal analysis, Data curation, Conceptualization. **Benoit Chachuat:** Writing – review & editing, Visualization, Validation, Supervision, Methodology. **Sihem Tebbani:** Writing – review & editing, Validation, Supervision, Software. **Olivier Bernard:** Writing – review & editing, Supervision, Software, Data curation, Conceptualization. **Filipa Lopes:** Writing – review & editing, Supervision, Project administration, Funding acquisition, Conceptualization.

Funding

This project has received funding from the European Union's Horizon 2020 Research and Innovation program under the Marie Skłodowska-Curie grant agreement No. 955520 DigitAlgaesation.

Declaration of competing interest

The authors declare no conflict of interest. The funders had no role in the design of the study; in the collection, analyses, or interpretation of data; in the writing of the manuscript, or in the decision to publish the results.

Acknowledgments

The authors would like to thank the program Horizon 2020 for fundings, and the ANR projects (French National Research Agency) Alligator, PhotobiofilmExplorer, MoBioSens and the “Fondation des Treilles” for sustaining their research.

Appendix A. Supplementary data

Supplementary data to this article can be found online at https://doi.org/10.1016/j.algal.2025.104201.

Data availability

Data will be made available on request.

References

[1] K.H. Halsey, B.M. Jones, Phytoplankton strategies for photosynthetic energy allocation, Ann. Rev. Mar. Sci. 7 (2015) 265–297, https://doi.org/10.1146/annurev-marine-010814-015813.
[2] J.A. Raven, R.J. Geider, Adaptation, acclimation and regulation in algal photosynthesis, in: A.W.D. Larkum, S.E. Douglas, J.A. Raven (Eds.), Photosynthesis in Algae, Springer Netherlands, Dordrecht, 2003, pp. 385–412, https://doi.org/10.1007/978-94-007-1038-2_17.
[3] K.J. Flynn, M. St John, J.A. Raven, D.O.F. Skibinski, J.I. Allen, A. Mitra, E. E. Hofmann, Acclimation, adaptation, traits and trade-offs in plankton functional type models: reconciling terminology for biology and modelling, J. Plankton Res. 37 (2015) 683–691, https://doi.org/10.1093/plankt/fbv036.
[4] M.A. Borowitzka, High-value products from microalgae—their development and commercialisation, J. Appl. Phycol. 25 (2013) 743–756, https://doi.org/10.1007/s10811-013-9983-9.
[5] Lee, C.-C. Microbial production of Astaxanthin, in: Jafari, S.M., Harzevili, F.D. (Eds.), Microbial Production of Food Bioactive Compounds. Springer International Publishing, Cham, 2022: pp. 1–38. https://doi.org/10.1007/978-3-030-81403-8_37-1 (accessed July 17, 2024).
[6] S. Boussiba, Carotenogenesis in the green alga *Haematococcus pluvialis*: cellular physiology and stress response, Physiol. Plant. 108 (2000) 111–117, https://doi.org/10.1034/j.1399-3054.2000.108002111.x.
[7] T. Roach, N. Böck, N. Rittmeier, E. Arc, I. Kranner, A. Holzinger, Acquisition of desiccation tolerance in *Haematococcus pluvialis* requires photosynthesis and coincides with lipid and astaxanthin accumulation, Algal Research 64 (2022) 102699, https://doi.org/10.1016/j.algal.2022.102699.
[8] X. Li, X. Wang, C. Duan, S. Yi, Z. Gao, C. Xiao, S.N. Agathos, G. Wang, J. Li, Biotechnological production of astaxanthin from the microalga *Haematococcus pluvialis*, Biotechnol. Adv. 43 (2020) 107602, https://doi.org/10.1016/j.biotechadv.2020.107602.
[9] M. Koller, A. Muhr, G. Braunegg, Microalgae as versatile cellular factories for valued products, Algal Res. 6 (2014) 52–63, https://doi.org/10.1016/j.algal.2014.09.002.
[10] J.H. Moreno Osorio, A. Pollio, L. Frunzo, P.N.L. Lens, G. Esposito, A review of microalgal biofilm technologies: definition, applications, settings and analysis, Front. Chem. Eng. 3 (2021), https://doi.org/10.3389/fceng.2021.737710.
[11] T.-T. Do, B.-N. Ong, T.-L. Le, T.-C. Nguyen, B.-H. Tran-Thi, B.T. Thu Hien, M. Melkonian, H.-D. Tran, Growth of *Haematococcus pluvialis* on a small-scale angled porous substrate Photobioreactor for green stage biomass, Appl. Sci. 11 (2021) 1788, https://doi.org/10.3390/app11041788.
[12] A.C. Kiperstok, P. Sebestyén, B. Podola, M. Melkonian, Biofilm cultivation of *Haematococcus pluvialis* enables a highly productive one-phase process for astaxanthin production using high light intensities, Algal Research 21 (2017) 213–222, https://doi.org/10.1016/j.algal.2016.10.025.
[13] D. Morgado, A. Fanesi, T. Martin, S. Tebbani, O. Bernard, F. Lopes, Exploring the dynamics of astaxanthin production in *Haematococcus pluvialis* biofilms using a

rotating biofilm-based system, Biotechnol. Bioeng. 121 (2023), https://doi.org/10.1002/bit.28624.
[14] H.-D. Tran, T.-T. Do, T.-L. Le, M.-L.T. Nguyen, C.-H. Pham, M. Melkonian, Cultivation of *Haematococcus pluvialis* for astaxanthin production on angled bench-scale and large-scale biofilm-based photobioreactors, Vietnam J. Sci. Technol. Eng. 61 (3) (2019) 61–70, https://doi.org/10.31276/VJSTE.61(3).61-70.
[15] M. Wan, D. Hou, Y. Li, J. Fan, J. Huang, S. Liang, W. Wang, R. Pan, J. Wang, S. Li, The effective photoinduction of *Haematococcus pluvialis* for accumulating astaxanthin with attached cultivation, Bioresour. Technol. 163 (2014) 26–32, https://doi.org/10.1016/j.biortech.2014.04.017.
[16] W. Zhang, J. Wang, J. Wang, T. Liu, Attached cultivation of *Haematococcus pluvialis* for astaxanthin production, Bioresour. Technol. 158 (2014) 329–335, https://doi.org/10.1016/j.biortech.2014.02.044.
[17] K.J. Flynn, R. Torres, X. Irigoien, J.C. Blackford, Plankton digital twins—a new research tool, J. Plankton Res. 44 (2022) 805, https://doi.org/10.1093/plankt/fbac042.
[18] F. Mairet, O. Bernard, Twelve quick tips for designing sound dynamical models for bioprocesses, PLoS Comput. Biol. 15 (2019) e1007222, https://doi.org/10.1371/journal.pcbi.1007222.
[19] P.G. Falkowski, J.A. Raven, Aquatic photosynthesis, Princeton University Press, 2013, https://doi.org/10.1515/9781400849727.
[20] M. Bekirogullari, G.M. Figueroa-Torres, J.K. Pittman, C. Theodoropoulos, Models of microalgal cultivation for added-value products - a review, Biotechnol. Adv. 44 (2020) 107609, https://doi.org/10.1016/j.biotechadv.2020.107609.
[21] O. Bernard, F. Mairet, B. Chachuat, Modelling of microalgae culture systems with applications to control and optimization, Adv. Biochem. Eng. Biotechnol. 153 (2016) 59–87, https://doi.org/10.1007/10_2014_287.
[22] A.W. Omta, J.D. Liefer, Z.V. Finkel, A.J. Irwin, D. Sher, M.J. Follows, A model of time-dependent macromolecular and elemental composition of phytoplankton, J. Theor. Biol. 592 (2024) 111883, https://doi.org/10.1016/j.jtbi.2024.111883.
[23] M.R. Mattei, L. Frunzo, B. D'Acunto, Y. Pechaud, F. Pirozzi, G. Esposito, Continuum and discrete approach in modeling biofilm development and structure: a review, J. Math. Biol. 76 (2018) 945–1003, https://doi.org/10.1007/s00285-017-1165-y.
[24] O. Wanner, H. Eberl, E. Morgenroth, D. Noguera, C. Picioreanu, B. Rittmann, M. van Loosdrecht, Mathematical Modeling of Biofilms, IWA Publishing, London, 2006, https://doi.org/10.2166/9781780402482.
[25] T. Li, B. Podola, M. Melkonian, Investigating dynamic processes in a porous substrate biofilm photobioreactor — a modeling approach, Algal Research 13 (2016) 30–40, https://doi.org/10.1016/j.algal.2015.11.006.
[26] T.E. Murphy, H. Berberoglu, Flux balancing of light and nutrients in a biofilm photobioreactor for maximizing photosynthetic productivity, Biotechnol. Prog. 30 (2014) 348–359, https://doi.org/10.1002/btpr.1881.
[27] L. Li, Y. Wang, L. Gao, W. Zhou, L. Chen, Z. Zhang, T. Liu, Experiments and cellular automata simulation reveal light/carbon transportation and growth mechanism of *Chlorella vulgaris* biofilm in attached cultivation, Chem. Eng. J. 457 (2023) 141177, https://doi.org/10.1016/j.cej.2022.141177.
[28] C. Luo, T. Long, Modeling microalgae biofilms morphology using a 2-D cellular automaton approach to reveal the combined effect of substrate and light, Algal Research 66 (2022) 102761, https://doi.org/10.1016/j.algal.2022.102761.
[29] B. Polizzi, A. Fanesi, F. Lopes, M. Ribot, O. Bernard, Understanding photosynthetic biofilm productivity and structure through 2D simulation, PLoS Comput. Biol. 18 (2022) e1009904, https://doi.org/10.1371/journal.pcbi.1009904.
[30] Md.M.R. Shah, Y. Liang, J.J. Cheng, M. Daroch, Astaxanthin-producing green microalga *Haematococcus pluvialis*: from single cell to high value commercial products, Front. Plant Sci. 7 (2016). https://www.frontiersin.org/articles/10.3389/fpls.2016.00531 (accessed January 3, 2023).
[31] A.E. Solovchenko, Recent breakthroughs in the biology of astaxanthin accumulation by microalgal cell, Photosynth. Res. 125 (2015) 437–449, https://doi.org/10.1007/s11120-015-0156-3.
[32] R. Luedeking, E.L. Piret, A kinetic study of the lactic acid fermentation. Batch process at controlled pH, J. Biochem. Microbiol. Technol. Eng. 1 (1959) 393–412, https://doi.org/10.1002/jbmte.390010406.
[33] E. Del Río, F.G. Acién, M.C. García-Malea, J. Rivas, E. Molina-Grima, M. G. Guerrero, Efficiency assessment of the one-step production of astaxanthin by the microalga *Haematococcus pluvialis*, Biotech & Bioengineering 100 (2008) 397–402, https://doi.org/10.1002/bit.21770.
[34] M.C. García-Malea, C. Brindley, E.D. Río, F.G. Acién, J.M. Fernández, E. Molina, Modelling of growth and accumulation of carotenoids in *Haematococcus pluvialis* as a function of irradiance and nutrients supply, Biochem. Eng. J. 26 (2005) 107–114, https://doi.org/10.1016/j.bej.2005.04.007.
[35] X.W. Zhang, X.-D. Gong, F. Chen, Kinetic models for astaxanthin production by high cell density mixotrophic culture of the microalga *Haematococcus pluvialis*, J. Ind. Microbiol. Biotechnol. 23 (1999) 691–696, https://doi.org/10.1038/sj.jim.2900685.
[36] E. Restiawaty, N.S. Salman, R. Maria, L.S. Broto, Y.W. Budhi, Modeling and simulation of astaxanthin production from Chlorella zofingiensis, Bioresource Technology Reports 25 (2024) 101722, https://doi.org/10.1016/j.biteb.2023.101722.
[37] D. Zhang, M. Wan, E.A. del Rio-Chanona, J. Huang, W. Wang, Y. Li, V. S. Vassiliadis, Dynamic modelling of *Haematococcus pluvialis* photoinduction for astaxanthin production in both attached and suspended photobioreactors, Algal Research 13 (2016) 69–78, https://doi.org/10.1016/j.algal.2015.11.019.
[38] M. Morales, H. Bonnefond, O. Bernard, Rotating algal biofilm versus planktonic cultivation: LCA perspective, J. Clean. Prod. (2020) 120547, https://doi.org/10.1016/j.jclepro.2020.120547.
[39] D. Penaranda, H. Bonnefond, F. Guihéneuf, M. Morales, O. Bernard, Life cycle assessment of an innovative rotating biofilm technology for microalgae production: an eco-design approach, J. Clean. Prod. 384 (2023) 135600, https://doi.org/10.1016/j.jclepro.2022.135600.
[40] O. Bara, H. Bonnefond, O. Bernard, Model development and light effect on a rotating algal biofilm, IFAC-PapersOnLine 52 (2019) 376–381, https://doi.org/10.1016/j.ifacol.2019.06.091.
[41] G.B. Jones, R.C. Sims, J. Zhao, Experimental and theoretical investigations of rotating algae biofilm reactors (RABRs): areal productivity, nutrient recovery, and energy efficiency, Biotechnol. Bioeng. (2023), https://doi.org/10.1002/bit.28451.
[42] R.J. Geider, H.L. MacIntyre, T.M. Kana, A dynamic regulatory model of phytoplanktonic acclimation to light, nutrients, and temperature, Limnol. Oceanogr. 43 (1998) 679–694, https://doi.org/10.4319/lo.1998.43.4.0679.
[43] M. Janssen de M. Winter J. Tramper L.R. Mur J. Snel R.H. Wijffels Efficiency of light utilization of *Chlamydomonas reinhardtii* under medium-duration light/dark cycles J. Biotechnol. 78 2000 123 137 https://doi.org/10.1016/s0168-1656(99)00233-3.
[44] E. Sforza, D. Simionato, G.M. Giacometti, A. Bertucco, T. Morosinotto, Adjusted light and dark cycles can optimize photosynthetic efficiency in algae growing in Photobioreactors, PloS One 7 (2012) e38975, https://doi.org/10.1371/journal.pone.0038975.
[45] A.E. Toninelli, J. Wang, M. Liu, H. Wu, T. Liu, *Scenedesmus dimorphus* biofilm: photoefficiency and biomass production under intermittent lighting, Sci. Rep. 6 (2016) 32305, https://doi.org/10.1038/srep32305.
[46] J.I. Fierro Ulloa, L.-D. Lu, O. Bernard, Theoretical growth rate of microalgae under high/low-flashing light, J. Math. Biol. 86 (2023) 48, https://doi.org/10.1007/s00285-023-01871-2.
[47] C. Combe, P. Hartmann, S. Rabouille, A. Talec, O. Bernard, A. Sciandra, Long-term adaptive response to high-frequency light signals in the unicellular photosynthetic eukaryote *Dunaliella salina*, Biotechnol. Bioeng. 112 (2015) 1111–1121, https://doi.org/10.1002/bit.25526.
[48] L. Pilon, R. Kandilian, Interaction between light and photosynthetic microorganisms, in: Advances in Chemical Engineering, Elsevier, 2016, pp. 107–149, https://doi.org/10.1016/bs.ache.2015.12.002.
[49] S. Ma, Y. Huang, B. Zhang, X. Zhu, A. Xia, X. Zhu, Q. Liao, Comprehensive modeling and predicting light transmission in microalgal biofilm, J. Environ. Manage. 326 (2023) 116757, https://doi.org/10.1016/j.jenvman.2022.116757.
[50] M.R. Droop, Vitamin B12 and marine ecology. IV. The kinetics of uptake, growth and inhibition in *Monochrysis Lutheri*, J. Mar. Biol. Assoc. U. K. 48 (1968) 689–733, https://doi.org/10.1017/S0025315400019238.
[51] M.R. Droop, 25 years of algal growth kinetics a personal view 26 (1983) 99–112, https://doi.org/10.1515/botm.1983.26.3.99.
[52] O. Bernard, Hurdles and challenges for modelling and control of microalgae for CO_2 mitigation and biofuel production, J. Process Control 21 (2011) 1378–1389, https://doi.org/10.1016/j.jprocont.2011.07.012.
[53] O. Bernard, J.-L. Gouzé, Transient behavior of biological loop models with application to the Droop model, Math. Biosci. 127 (1995) 19–43, https://doi.org/10.1016/0025-5564(94)00040-7.
[54] M. Cherif, M. Loreau, Towards a more biologically realistic use of Droop's equations to model growth under multiple nutrient limitation, Oikos 119 (2010) 897–907, https://doi.org/10.1111/j.1600-0706.2010.18397.x.
[55] O. Bernard, B. Rémond, Validation of a simple model accounting for light and temperature effect on microalgal growth, Bioresour. Technol. 123 (2012) 520–527, https://doi.org/10.1016/j.biortech.2012.07.022.
[56] H.L. MacIntyre, T.M. Kana, T. Anning, R.J. Geider, Photoacclimation of photosynthesis irradiance response curves and photosynthetic pigments in microalgae and Cyanobacteria1, J. Phycol. 38 (2002) 17–38, https://doi.org/10.1046/j.1529-8817.2002.00094.x.
[57] D. Demory, C. Combe, P. Hartmann, A. Talec, E. Pruvost, R. Hamouda, F. Souillé, P.-O. Lamare, M.-O. Bristeau, J. Sainte-Marie, S. Rabouille, F. Mairet, A. Sciandra, O. Bernard, How do microalgae perceive light in a high-rate pond? Towards more realistic Lagrangian experiments, R. Soc. Open Sci. 5 (2018) 180523, https://doi.org/10.1098/rsos.180523.
[58] M.H. Huesemann, J. Van Wagenen, T. Miller, A. Chavis, S. Hobbs, B. Crowe, A screening model to predict microalgae biomass growth in photobioreactors and raceway ponds, Biotechnol. Bioeng. 110 (2013) 1583–1594, https://doi.org/10.1002/bit.24814.
[59] J. Huisman, H.C.P. Matthijs, P.M. Visser, H. Balke, C.A.M. Sigon, J. Passarge, F. J. Weissing, L.R. Mur, Principles of the light-limited chemostat: theory and ecological applications, Antonie Van Leeuwenhoek 81 (2002) 117–133, https://doi.org/10.1023/a:1020537928216.
[60] A.M. Collins, H.D.T. Jones, D. Han, Q. Hu, T.E. Beechem, J.A. Timlin, Carotenoid distribution in living cells of *Haematococcus pluvialis* (Chlorophyceae), PloS One 6 (2011) e24302, https://doi.org/10.1371/journal.pone.0024302.
[61] S. Ota, A. Morita, S. Ohnuki, A. Hirata, S. Sekida, K. Okuda, Y. Ohya, S. Kawano, Carotenoid dynamics and lipid droplet containing astaxanthin in response to light in the green alga *Haematococcus pluvialis*, Sci. Rep. 8 (2018) 5617, https://doi.org/10.1038/s41598-018-23854-w.
[62] M. Wayama, S. Ota, H. Matsuura, N. Nango, A. Hirata, S. Kawano, Three-dimensional ultrastructural study of oil and Astaxanthin accumulation during Encystment in the green alga *Haematococcus pluvialis*, PloS One 8 (2013) e53618, https://doi.org/10.1371/journal.pone.0053618.

[63] L. Fang, J. Zhang, Z. Fei, M. Wan, Chlorophyll as key indicator to evaluate astaxanthin accumulation ability of *Haematococcus pluvialis*, Bioresour. Bioprocess. 6 (2019) 52, https://doi.org/10.1186/s40643-019-0287-z.

[64] O. Bernard, P. Masci, A. Sciandra, A photobioreactor model in nitrogen limited conditions, in: Mathmod 09 - 6th Vienna International Conference on Mathematical Modelling, Vienne, Austria, 2009 https://hal.science/hal-03523391 (accessed June 19, 2024).

[65] C.S. Reynolds, S.C. Maberly, A simple method for approximating the supportive capacities and metabolic constraints in lakes and reservoirs, Freshw. Biol. 47 (2002) 1183–1188, https://doi.org/10.1046/j.1365-2427.2002.00839.x.

[66] A.C. Kiperstok, Optimizing Immobilized Cultivation of *Haematococcus pluvialis* for Astaxanthin Production, Universität zu Köln, 2016 https://kups.ub.uni-koeln.de/6728/.

[67] S.P. Asprey, S. Macchietto, Statistical tools for optimal dynamic model building, Comput. Chem. Eng. 24 (2000) 1261–1267, https://doi.org/10.1016/S0098-1354(00)00328-8.

[68] P.G. Falkowski, C.D. Wirick, A simulation model of the effects of vertical mixing on primary productivity, Mar. Biol. 65 (1981) 69–75, https://doi.org/10.1007/BF00397069.

[69] F. Mairet, O. Bernard, T. Lacour, A. Sciandra, Modelling microalgae growth in nitrogen limited photobiorector for estimating biomass, carbohydrate and neutral lipid productivities, IFAC Proceedings Volumes 44 (2011) 10591–10596, https://doi.org/10.3182/20110828-6-IT-1002.03165.

[70] Q. Béchet, A. Shilton, B. Guieysse, Modeling the effects of light and temperature on algae growth: state of the art and critical assessment for productivity prediction during outdoor cultivation, Biotechnol. Adv. 31 (2013) 1648–1663, https://doi.org/10.1016/j.biotechadv.2013.08.014.

[71] H.C. Bernstein, M. Kesaano, K. Moll, T. Smith, R. Gerlach, R.P. Carlson, C. D. Miller, B.M. Peyton, K.E. Cooksey, R.D. Gardner, R.C. Sims, Direct measurement and characterization of active photosynthesis zones inside wastewater remediating and biofuel producing microalgal biofilms, Bioresour. Technol. 156 (2014) 206–215, https://doi.org/10.1016/j.biortech.2014.01.001.

[72] T. Li, B. Piltz, B. Podola, A. Dron, D. de Beer, M. Melkonian, Microscale profiling of photosynthesis-related variables in a highly productive biofilm photobioreactor, Biotechnol. Bioeng. 113 (2016) 1046–1055, https://doi.org/10.1002/bit.25867.

[73] L.-L. Zhuang, W. Tian, Y. Yang, S. Ge, P. Li, S. Sun, J. Zhang, S. Liang, Quantified trend of photosynthetic rate along the depth of microalgae biofilm, Sci. Total Environ. 876 (2023) 162801, https://doi.org/10.1016/j.scitotenv.2023.162801.

[74] P.J. Schnurr, G.S. Espie, D.G. Allen, The effect of light direction and suspended cell concentrations on algal biofilm growth rates, Appl. Microbiol. Biotechnol. 98 (2014) 8553–8562, https://doi.org/10.1007/s00253-014-5964-4.

[75] S.T. Chua, A. Smith, S. Murthy, M. Murace, H. Yang, L. Schertel, M. Kühl, P. Cicuta, A.G. Smith, D. Wangpraseurt, S. Vignolini, Light management by algal aggregates in living photosynthetic hydrogels, Proc. Natl. Acad. Sci. 121 (2024) e2316206121, https://doi.org/10.1073/pnas.2316206121.

[76] J. Grenier, H. Bonnefond, F. Lopes, O. Bernard, The impact of light supply to moving photosynthetic biofilms, Algal Research 44 (2019) 101674, https://doi.org/10.1016/j.algal.2019.101674.

[77] D. Morgado, A. Fanesi, T. Martin, S. Tebbani, O. Bernard, F. Lopes, Non-destructive monitoring of microalgae biofilms, Bioresour. Technol. 398 (2024) 130520, https://doi.org/10.1016/j.biortech.2024.130520.

[78] W. Blanken, M. Janssen, M. Cuaresma, Z. Libor, T. Bhaiji, R.H. Wijffels, Biofilm growth of *Chlorella sorokiniana* in a rotating biological contactor based photobioreactor: biofilm growth of *Chlorella sorokiniana*, Biotechnol. Bioeng. 111 (2014) 2436–2445, https://doi.org/10.1002/bit.25301.

[79] J.T. Lehman, D.B. Botkin, G.E. Likens, The assumptions and rationales of a computer model of phytoplankton population dynamics1, Limnol. Oceanogr. 20 (1975) 343–364, https://doi.org/10.4319/lo.1975.20.3.0343.

[80] C.S. Reynolds, The Ecology of Phytoplankton, Cambridge University Press, Cambridge, 2006, https://doi.org/10.1017/CBO9780511542145.

[81] G. Wolf, C. Picioreanu, M.C.M. van Loosdrecht, Kinetic modeling of phototrophic biofilms: the PHOBIA model, Biotechnol. Bioeng. 97 (2007) 1064–1079, https://doi.org/10.1002/bit.21306.

[82] O. Ross, R. Geider, New cell-based model of photosynthesis and photo-acclimation: accumulation and mobilisation of energy reserves in phytoplankton, Mar. Ecol. Prog. Ser. 383 (2009) 53–71, https://doi.org/10.3354/meps07961.

[83] D.-K. Kim, S.-J. Hong, J.-H. Bae, N. Yim, E. Jin, C.-G. Lee, Transcriptomic analysis of *Haematococcus lacustris* during astaxanthin accumulation under high irradiance and nutrient starvation, Biotechnol Bioproc E 16 (2011) 698–705, https://doi.org/10.1007/s12257-011-0081-z.

[84] L. Recht, N. Töpfer, A. Batushansky, N. Sikron, Y. Gibon, A. Fait, Z. Nikoloski, S. Boussiba, A. Zarka, Metabolite profiling and integrative modeling reveal metabolic constraints for carbon partitioning under nitrogen starvation in the green algae *Haematococcus pluvialis*, J. Biol. Chem. 289 (2014) 30387–30403, https://doi.org/10.1074/jbc.M114.555144.

[85] L. Scibilia, L. Girolomoni, S. Berteotti, A. Alboresi, M. Ballottari, Photosynthetic response to nitrogen starvation and high light in *Haematococcus pluvialis*, Algal Research 12 (2015) 170–181, https://doi.org/10.1016/j.algal.2015.08.024.

[86] M. Gross, D. Jarboe, Z. Wen, Biofilm-based algal cultivation systems, Appl. Microbiol. Biotechnol. 99 (2015) 5781–5789, https://doi.org/10.1007/s00253-015-6736-5.

[87] M.B. Johnson, Z. Wen, Development of an attached microalgal growth system for biofuel production, Appl. Microbiol. Biotechnol. 85 (2010) 525–534, https://doi.org/10.1007/s00253-009-2133-2.

[88] L. Fan, A. Vonshak, S. Boussiba, Effect of temperature and irradiance on growth of *Haematococcus Pluvialis* (chlorophyceae)1, J. Phycol. 30 (1994) 829–833, https://doi.org/10.1111/j.0022-3646.1994.00829.x.

[89] C. Hagen, K. Grünewald, S. Schmidt, J. Müller, Accumulation of secondary carotenoids in flagellates of *Haematococcus pluvialis* (Chlorophyta) is accompanied by an increase in per unit chlorophyll productivity of photosynthesis, Eur. J. Phycol. 35 (2000) 75–82, https://doi.org/10.1080/09670260010001735651.

[90] K.J. Flynn, The importance of the form of the quota curve and control of non-limiting nutrient transport in phytoplankton models, J. Plankton Res. 30 (2008) 423–438, https://doi.org/10.1093/plankt/fbn007.

[91] A. Nikolaou, P. Hartmann, A. Sciandra, B. Chachuat, O. Bernard, Dynamic coupling of photoacclimation and photoinhibition in a model of microalgae growth, J. Theor. Biol. 390 (2016) 61–72, https://doi.org/10.1016/j.jtbi.2015.11.004.

[92] A.E. Solovchenko, O.B. Chivkunova, I.P. Maslova, Pigment composition, optical properties, and resistance to photodamage of the microalga *Haematococcus pluvialis* cultivated under high light, Russ. J. Plant Physiol. 58 (2011) 9–17, https://doi.org/10.1134/S1021443710061056.

[93] G. Panis, J.R. Carreon, Commercial astaxanthin production derived by green alga *Haematococcus pluvialis*: a microalgae process model and a techno-economic assessment all through production line, Algal Research 18 (2016) 175–190, https://doi.org/10.1016/j.algal.2016.06.007.

[94] E. Del Río, F.G. Acién, M.C. García-Malea, J. Rivas, E. Molina-Grima, M. G. Guerrero, Efficient one-step production of astaxanthin by the microalga Haematococcus pluvialis in continuous culture, Biotechnol. Bioeng. 91 (2005) 808–815, https://doi.org/10.1002/bit.20547.

[95] M.C. García-Malea, F.G. Acién, J.M. Fernández, M.C. Cerón, E. Molina, Continuous production of green cells of *Haematococcus pluvialis*: modeling of the irradiance effect, Enzyme Microb. Technol. 38 (2006) 981–989, https://doi.org/10.1016/j.enzmictec.2005.08.031.

[96] M.C. García-Malea, F.G. Acién, E. Del Río, J.M. Fernández, M.C. Cerón, M. G. Guerrero, E. Molina-Grima, Production of astaxanthin by *Haematococcus pluvialis*: taking the one-step system outdoors, Biotechnol. Bioeng. 102 (2009) 651–657, https://doi.org/10.1002/bit.22076.

[97] L. Recht, A. Zarka, S. Boussiba, Patterns of carbohydrate and fatty acid changes under nitrogen starvation in the microalgae *Haematococcus pluvialis* and *Nannochloropsis sp*, Appl. Microbiol. Biotechnol. 94 (2012) 1495–1503, https://doi.org/10.1007/s00253-012-3940-4.

[98] L. Recht, N. Töpfer, A. Batushansky, N. Sikron, Y. Gibon, A. Fait, Z. Nikoloski, S. Boussiba, A. Zarka, Metabolite profiling and integrative modeling reveal metabolic constraints for carbon partitioning under nitrogen starvation in the green algae *Haematococcus pluvialis*, J. Biol. Chem. 289 (2014) 30387–30403, https://doi.org/10.1074/jbc.M114.555144.

[99] G. Chen, B. Wang, D. Han, M. Sommerfeld, Y. Lu, F. Chen, Q. Hu, Molecular mechanisms of the coordination between astaxanthin and fatty acid biosynthesis in Haematococcus pluvialis (Chlorophyceae), Plant J. 81 (2015) 95–107, https://doi.org/10.1111/tpj.12713.

[100] K. Chekanov, E. Schastnaya, K. Neverov, S. Leu, S. Boussiba, A. Zarka, A. Solovchenko, Non-photochemical quenching in the cells of the carotenogenic chlorophyte *Haematococcus lacustris* under favorable conditions and under stress, Biochim. Biophys. Acta Gen. Subj. 1863 (2019) 1429–1442, https://doi.org/10.1016/j.bbagen.2019.05.002.

[101] K. Samhat, A. Kazbar, H. Takache, A. Ismail, J. Pruvost, Influence of light absorption rate on the astaxanthin production by the microalga *Haematococcus pluvialis* during nitrogen starvation, Bioresour. Bioprocess. 10 (2023) 78, https://doi.org/10.1186/s40643-023-00700-0.

[102] K. Samhat, A. Kazbar, H. Takache, O. Gonçalves, D. Drouin, A. Ismail, J. Pruvost, Optimization of continuous astaxanthin production by *Haematococcus pluvialis* in nitrogen-limited photobioreactor, Algal Research 80 (2024) 103529, https://doi.org/10.1016/j.algal.2024.103529.

[103] E.G. Baroni, K.Y. Yap, P.A. Webley, P.J. Scales, G.J.O. Martin, The effect of nitrogen depletion on the cell size, shape, density and gravitational settling of *Nannochloropsis salina*, *Chlorella* sp. (marine) and *Haematococcus pluvialis*, Algal Res. 39 (2019) 101454, https://doi.org/10.1016/j.algal.2019.101454.

[104] A. Usai, J.K. Pittman, C. Theodoropoulos, A multiscale modelling approach for *Haematococcus pluvialis* cultivation under different environmental conditions, Biotechnology Reports 36 (2022) e00771, https://doi.org/10.1016/j.btre.2022.e00771.

[105] D.L. Reinecke, A. Castillo-Flores, S. Boussiba, A. Zarka, Polyploid polynuclear consecutive cell-cycle enables large genome-size in *Haematococcus pluvialis*, Algal Research 33 (2018) 456–461, https://doi.org/10.1016/j.algal.2018.06.013.

[106] C. Zhang, J. Liu, L. Zhang, Cell cycles and proliferation patterns in Haematococcus pluvialis, Chin. J. Ocean. Limnol. 35 (2017) 1205–1211, https://doi.org/10.1007/s00343-017-6103-8.

[107] M. Kesaano, R.D. Gardner, K. Moll, E. Lauchnor, R. Gerlach, B.M. Peyton, R. C. Sims, Dissolved inorganic carbon enhanced growth, nutrient uptake, and lipid accumulation in wastewater grown microalgal biofilms, Bioresour. Technol. 180 (2015) 7–15, https://doi.org/10.1016/j.biortech.2014.12.082.

[108] I. López Muñoz, O. Bernard, Modeling the influence of temperature, light intensity and oxygen concentration on microalgal growth rate, Processes 9 (2021) 496, https://doi.org/10.3390/pr9030496.

[109] E. Sforza, M. Pastore, S.M. Franke, E. Barbera, Modeling the oxygen inhibition in microalgae: an experimental approach based on photorespirometry, N. Biotechnol. 59 (2020) 26–32, https://doi.org/10.1016/j.nbt.2020.06.003.

[110] D. de Beer, V. Meyer, J. Klatt, T. Li, Photosynthesis Under Very High Oxygen Concentrations in Dense Microbial Mats and Biofilms, 2018, https://doi.org/10.1101/335299.
[111] M. Kobayashi, Astaxanthin biosynthesis enhanced by reactive oxygen species in the green alga *Haematococcus pluvialis*, Biotechnol. Bioprocess Eng. 8 (2003) 322–330, https://doi.org/10.1007/BF02949275.
[112] Q. Li, L. Li, Y. Zhang, H. Gao, Y. Zhao, X. Yu, Chemical inducers regulate ROS signalling to stimulate astaxanthin production in *Haematococcus pluvialis* under environmental stresses: a review, Trends Food Sci. Technol. 136 (2023) 181–193, https://doi.org/10.1016/j.tifs.2023.04.014.
[113] P.-O. Lamare, N. Aguillon, J. Sainte-Marie, J. Grenier, H. Bonnefond, O. Bernard, Gradient-based optimization of a rotating algal biofilm process, Automatica 105 (2019) 80–88, https://doi.org/10.1016/j.automatica.2019.02.043.
[114] L. Giannelli, H. Yamada, T. Katsuda, H. Yamaji, Effects of temperature on the astaxanthin productivity and light harvesting characteristics of the green alga *Haematococcus pluvialis*, J. Biosci. Bioeng. 119 (2015) 345–350, https://doi.org/10.1016/j.jbiosc.2014.09.002.
[115] A. Fratamico, P. Tocquin, F. Franck, The chlorophyll a fluorescence induction curve in the green microalga *Haematococcus pluvialis*: further insight into the nature of the P–S–M fluctuation and its relationship with the "low-wave" phenomenon at steady-state, Photosynth. Res. 128 (2016) 271–285, https://doi.org/10.1007/s11120-016-0241-2.
[116] C. Aflalo, Y. Meshulam, A. Zarka, S. Boussiba, On the relative efficiency of two- vs. one-stage production of astaxanthin by the green alga *Haematococcus pluvialis*, Biotechnol. Bioeng. 98 (2007) 300–305, https://doi.org/10.1002/bit.21391.
[117] J.D. Liefer, A. Garg, D.A. Campbell, A.J. Irwin, Z.V. Finkel, Nitrogen starvation induces distinct photosynthetic responses and recovery dynamics in diatoms and prasinophytes, PloS One 13 (2018) e0195705, https://doi.org/10.1371/journal.pone.0195705.
[118] K. Chekanov, A. Lukyanov, S. Boussiba, C. Aflalo, A. Solovchenko, Modulation of photosynthetic activity and photoprotection in *Haematococcus pluvialis* cells during their conversion into haematocysts and back, Photosynth. Res. 128 (2016) 313–323, https://doi.org/10.1007/s11120-016-0246-x.
[119] P.P. Patil, K. Nagy, Á. Ábrahám, I. Vass, M. Szabó, Monitoring the photosynthetic activity at single-cell level in *Haematococcus lacustris*, Photosynt 61 (2023) 473–482, https://doi.org/10.32615/ps.2023.042.
[120] A. Fanesi, M. Lavayssière, C. Breton, O. Bernard, R. Briandet, F. Lopes, Shear stress affects the architecture and cohesion of Chlorella vulgaris biofilms, Sci. Rep. 11 (2021) 4002, https://doi.org/10.1038/s41598-021-83523-3.
[121] P.J. Schnurr, G.S. Espie, G.D. Allen, The effect of photon flux density on algal biofilm growth and internal fatty acid concentrations, Algal Research 16 (2016) 349–356, https://doi.org/10.1016/j.algal.2016.04.001.
[122] X. Li, X. Wang, C. Duan, S. Yi, Z. Gao, C. Xiao, S.N. Agathos, G. Wang, J. Li, Biotechnological production of astaxanthin from the microalga *Haematococcus pluvialis*, Biotechnol. Adv. 43 (2020) 107602, https://doi.org/10.1016/j.biotechadv.2020.107602.
[123] G.B. Jones, R.C. Sims, J. Zhao, Computational modeling of microalgal biofilm growth in heterogeneous rotating algal biofilm reactors (RABRs) for wastewater treatment, App. Math. Model. 131 (2024) 487–504, https://doi.org/10.1016/j.apm.2024.04.021.
[124] Alexander Schaum, Marta Mandis, Pascal Jerono, Stefania Tronci, Thomas Meurer, State estimation of microalgae photobioreactors: applications to *Haematococcus pluvialis*, Chem. Eng. Trans. 74 (2019) 1423–1428, https://doi.org/10.3303/CET1974238.